OREGON HEALTH & SCIENCE UNIVERSITY
SCHOOL OF MEDICINE – GRADUATE STUDIES

Evaluation and Optimization of Injected Activity and Scan Time on a 3 and 5-ring GE PET/CT While Maintaining Clinical Image Quality

By
Zahra Sadat Mojabi

A THESIS

Presented to
Oregon Health & Science University
School of Medicine
in partial fulfillment of
the requirements for the degree of
Master of Science

Presented June, 2021

OREGON HEALTH & SCIENCE UNIVERSITY
SCHOOL OF MEDICINE – GRADUATE STUDIES

School of Medicine

Oregon Health & Science University

CERTIFICATE OF APPROVAL

This is to certify that the Master's thesis of

Zahra Sadat Mojabi

has been approved

Mentor/Advisor

Member

Member

Member

TABLE OF CONTENTS

List of Figures

List of Tables

Acknowledgments

I would like to express my appreciation to the faculty and staff of Oregon Health and Science University for the high level of education that I received in the field of Medical Physics that encouraged me to continue my career in the future.

I also would like to express the deepest sincerity to my thesis committee members including Dr. Thomas Griglock, Dr. Anna Mench, Dr. Anderi Pugachev, and Mr. Isaac Bailey. Thank you for your support, help, and advice throughout the classroom, my thesis, Ph. D. applications, interview process, and future career. In addition, I would like to express my great thank you to Dr. Lindsay DeWeese for her support, advice, motivation, and help in the classroom, my Ph. D. applications, interview process, and future career.

This dissertation and research would also not have been possible without the help of Mr. Bailey. A debt of gratitude is also owed to him for advising and supporting me toward the thesis and providing me with guidance for my research.

Last but not least, I would like to acknowledge with gratitude the support and love of my parents, my brother, and my sisters and that without their consistent encouragement and advice, none of this would indeed be possible.

Finally, I thank everyone for all your support, encouragement, and help during my graduate school.

Abstract:

Introduction: PET image data is regularly reconstructed with iterative techniques, including the maximum likelihood-expectation maximization (MLEM) and the ordered-subset expectation maximization (OSEM) methods. GE Healthcare has introduced a new reconstruction technique known as Q. Clear with a penalization factor (β) in order to improve the image quality (IQ) parameters and qualification of PET data. This study compared the IQ impact of our facility's current clinical OSEM (C. OSEM) and the available Q. Clear reconstruction technique using a NEMA phantom. We investigated the optimum β value and its effect on IQ parameters on our 3 and 5-ring PET/CT scanners that would maintain the current diagnostic level of IQ while possibly allowing for a decrease in scan time on the scanners.

Method: The phantom's spheres with various diameters were used to simulate hot and cold lesions. On both scanners, the NEMA image-quality phantom was scanned with an FDG concentration ratio in the hot spheres to background of 4:1 following the instructions of NEMA IQ testing from the vendor. The PET data was reconstructed with various scan times (1-6 minutes) with different reconstruction techniques including OSEM of vendor procedure, C. OSEM, and Q. Clear with various β values (300, 400, 500, 600, and 1000). Our C. OSEM reconstruction technique with 2.5 min bed position (bp) was used as our standard to which we would compare the other simulated reconstructions. IQ parameters including contrast recovery (CR), background variability (BV), and contrast to noise ratio (CNR=CR/BV) were measured on a single frame scan for every reconstructed technique at the various scan times.

Result: On the 3-ring scanner, the CR and BV decreased with increasing β values at each simulated scan time for all spheres, while increasing scan time led to an increase in the CNR for all spheres. The CR and BV with the C. OSEM reconstruction were lower than the CR and BV of the OSEM technique, but the CNR of C. OSEM was higher than the CNR of the GE's standard NEMA OSEM reconstruction. On the 5-ring system, increasing the β values at various scan times resulted in a decrease in the CR and BV values, with an increase in CNR. On the 5 ring system, the C. OSEM CR, BV, and CNR values were lower than the CR, BV, and CNR values reconstructed by Q. Clear for β values of 500 and 600 and 2 and 2.5 min/bp. Comparing the C. OSEM 2.5 min/bp on the 3-ring scanner with the Q. Clear reconstruction on the 5-ring scanner demonstrated that the IQ parameters were higher for β values of 300, 400, 500, 600, and 1000 at 2 and 2.5 min/bp.

Conclusion: Our results illustrate that the C.OSEM with 2.5 min/bp on our facility's 3-ring detector PET/CT has been well optimized. On the PET/CT with a 5-ring detector, the Q. Clear reconstruction with a β value of 500 and a 2 min/bp provided higher IQ parameters. Then, a decrease in scan time may be possible on the 5-ring PET/CT system while meeting current clinical IQ standards.

1. Introduction

The medical physics field is based on applying physics principles to medicine and patient care to improve healthcare through diagnostic imaging and radiation therapy. Specifically in diagnostic imaging, where patient safety is a major priority, responsibilities include making sure the imaging protocols are regularly optimized and the diagnostic imaging units passed the quality control and quality assurance tests (1). According to our responsibilities, the physicist needs to be educated in physics, medicine, and the applications of each imaging modality with respect to patient safety and acquiring a high diagnostic quality image. We aim to optimize ionizing radiation from the imaging protocols while the image quality is kept at a diagnostic level. Since 2006 (2), hybrid modalities such as PET/CT are growing in popularity in medical imaging. It is beneficial to diagnose the disease earlier with both anatomical and functional imaging units. However, the $^{18}F-FDG$ PET scan shows the accuracies range from 80% to 90% to diagnose, stage, and restage many types of cancer (3), there is a concern to optimize the administered radionuclide or scan time to decrease the patient dose while the image quality will be preserved.

Over time, the manufactures of the PET scanners have developed these systems with advanced detector materials, advanced image reconstruction techniques, and larger field of views (FOV) to pursue a balance the administered dose with the image quality. On a specific PET unit, this effort would be evaluated by the healthcare professional including the medical physicist, the technologist, and radiologist. The physical and image reconstruction improvements of PET scans presented the possibility of optimization of administered radionuclide and scan time, while ensuring the image quality is at an acceptable level. Common image reconstruction techniques of PET image data include the Ordered Subset Expectation Maximization (OSEM), Point Spread

Function (PSF), and Time-Of- Flight (TOF) methods. A recent improvement of image reconstruction techniques is known as Bayesian Panelized Likelihood (BPL) reconstruction, which GE Healthcare calls Q. Clear on their PET systems (4, 5). The typical axial FOV size of the PET scanner was 15 cm, then it increased to 20 cm, and with the recent advancement of PET scanners, the axial FOV of 25 cm is available. GE Healthcare's PET/CT unit is known as the GE Discovery MI PET/CT and systems available with 3, 4 and 5-ring detector configurations for 15, 20 , and 25 cm FOVs respectively (6). One of the PET Units evaluated in this study has 3-rings of detectors with the PET scanning FOV of 15 cm, and the other one has 5-rings of detectors with a FOV of 25 cm. The 5-ring PET/CT Discovery MI (25 cm FOV) is located on the 4th floor of Peter O. Kohler Pavilion in the Radiation Medicine Department of the University Hospital on OHSU's main campus. The 3-ring PET/CT Discovery MI (15 cm FOV) is located at OHSU's Knight Cancer Institute clinic in Beaverton, OR. As there are two units at Oregon Health and Science University (OHSU), the main aim of this study is to take an advantage of the new image reconstruction technique and the greater FOV of the second scanner to optimize scan time (or injected activity).

The sensitivity of PET scanner will be improved by increasing the axial FOV of the scanner and also, the spatial resolution of the scanner depends on not only the type of photomultiplier tubes (PMTs) used with the detectors within 4-5 mm, but also it relates to both sensitivity and scan time (7). The improvement of spatial resolution requires a proportional improvement of the sensitivity (count per second) to preserve the image noise level (8). Furthermore, due to the larger axial FOV and replacement of conventional PMTs with more efficient silicon PMTs (SiPM), the sensitivity (up to 20 kcps/MBq) and coincidence timing resolution (in the range of 210-400 ps) were improved (6, 9, 10). Radionuclides have an exponential decay constant where the number of initial unstable atoms can decay to the stable position by emitting a gamma ray or particle (beta, alpha, and etc.).

The activity can be defined by the number of radionuclide can be transformed per second with the exponential formula. These physical improvements lead not only to a decrease of scan time (or injected activity) but also could decrease the respiratory motion artifacts of a PET scan. However, the short scan time of a PET scan would cause an increase in the statistical noise as the number of counts per second would decrease. Still, the advanced image reconstruction technique and large axial FOV could improve the image quality and suppress the increasing noise level.

The common reconstruction technique of PET image date is iterative algorithms, mostly OSEM. The modern PET scanner is equipped to perform TOF and PSF reconstruction techniques. The advantage of TOF is improving Signal-to-Noise ratio (SNR) at comparable convergence level (11) with no effect on standardized uptake values (SUV) (12). The benefit of PSF is increasing the reconstructed spatial resolution (13) and improving the SUV_{max} more than 30% in clinical research (14). While these reconstruction techniques are useful to make a tradeoff between the contrast recovery (CR) and SNR of PET data, the previous reconstruction techniques have a limitation that the SNR is decreased if the number of iteration or subsets were increased to achieve sufficient CR values (15). GE Healthcare's newer reconstruction technique is called Q. Clear which is a Bayesian Panelized likelihood reconstruction (BPL) method. Q. Clear creates a high SNR in uniform areas and full convergence of focal activity peaks within the same PET data (16). This technique contains PSF modeling and needs a user to define a penalization factor, called Beta (β), to use it as a voxel-wise regulation of the iterative steps. The Q. Clear technique contains a relative difference penalty (16), and the penalty function includes the difference between neighborhoods of each voxel and their sum (17). This penalty factor acts as a noise suppression term, and it is controlled by the value of β. The optimization of the Q. Clear algorithm is achieved with the modified block sequential regularized expectation maximization and because of the penalty function, an effective

convergence and accurate SUV could be achieved (17, 18). However, the contrast converge with the OSEM reconstruction technique could not be achieved because of the increased image noise (19, 20). Previous studies present the improvement image quality parameters of PET data by using the Q. Clear technique in both phantom and patient studies. The optimized value of β was 350 introduced by the vendor, but it is likely that the value would be varied based on the local hospital radiologist and radio-oncologist.

2. Aim of Study

The aim of this thesis was to evaluate the effect of implementing Q. Clear image reconstruction technique on both the 3 and 5-ring GE Discovery MI PET/CT units at Oregon Health and Science University (OHSU). The goal was to assess the possibility of decreasing scan time (or injected activity) on both systems while maintaining the current clinical image quality. NEMA Phantom analysis was performed on both scanners to evaluate the impact of Q. Clear reconstruction technique with various β values compared to the standard clinical image reconstruction technique (OSEM+TOF) at 2.5 min time per bed position (bp) on image quality parameters (IQ). Also, we investigated the effect of decreasing scan time to less than the clinical standard of 2.5 min on the IQ parameters. This study will hopefully be beneficial to the present patient protocol of PET scan by improving the clinical performance and possibly lowering the administered patient dose. The physics and medicine aspects of PET scans will be described in the background session of this thesis. This section will contain the details of the PET scanner, image reconstruction techniques, various radionuclides and their medical applications, radiation dose from CT and PET scans, and lastly, the CT component of PET/CT scanner. The background will be followed by the methods of this study, the achieved results, a discussion of the results, and the conclusions of this study.

3. Background

3.1 Positron Emission Tomography (PET)

Since the first positron tomography system was developed in the mid-1970s, there have been significant improvements in the technology, including the development of PET/CT systems (21). Over time, the scan time, reconstruction technique, detector material, dedicated radionuclide, and large axial field of view were implemented to PET/CT systems to improve the performance and reliability. These advancements were necessary since it was a first hybrid modality of both functional and anatomical diagnostic imaging. PET data is used to visualize and measure a diverse range of biological processes (22). This modality has a specific and sensitive definition of molecular imaging interaction within the body (23). Each positron-emitting radionuclide has their own positron range that can be used to specify the radionuclide and emitted radiation (22), which can be identified a PET imaging as metabolic and physiological imaging. PET is a sensitive imaging modality as its capability to detect the low molecular mass of radionuclide is dependent on two factors. First, the radionuclide is produced with labeled compounds with high specific activity, known as radiolabeled (22). Second, PET is equipped with coincidence counting to capture the paired annihilation of both photons with 511 keV energy that are emitted from positron annihilation with an electron, in this way PET can localize the local uptake and position of positron-emitter radionuclide within the anatomy (22).

PET systems have dedicated design concepts to capture the paired annihilation photons, including annihilation coincidence detection; true, random, and scatter coincidences; detection of interaction; scatter coincidence; three-dimensional data acquisition; and various data correction

techniques. That is all applied to PET data to obtain a diagnostic quality image. The detailed description of every PET design and concept is beyond the scope of this thesis, and the related aspects will be described in the following sections.

3.1.1 Coincidence Detection of Annihilation

A positron emitter radionuclide moves inside a human body and loses its kinetic energy by interaction with material through the excitation and ionization pathway. At the end of this pathway, the positron interacts with an electron through the annihilation process. This interaction occurs when the entire mass of the electron-positron pair is transformed into energy equal to 1.022 MeV. It appears as two photons with energy of 511 keV that are emitted in approximately opposite directions (Figure 1). Before this interaction, the travel range of positron is varied based on the type of radionuclides (F-18, O-15, N-13, and etc.) (24).

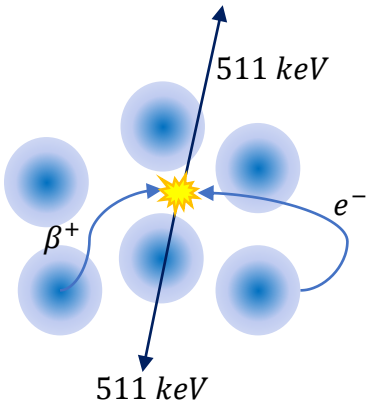

Figure 1. Annihilation process. When the positron interacts with the electron at the end of its pathway, then the entire their mass is transformed into energy equal to 1.022 MeV and it appears as two photons with energy of 511 keV that are emitted approximately opposite directions.

If these emitted annihilation photons simultaneously interact with the two detectors and the annihilation process happened close to the line connecting these detectors (Figure 2-A), the

detection is called Annihilation Coincidence Detection (ACD). Then, the scanner characterizes a line in the space between these detectors, known as the line of response (LOR). An ACD between these detectors determines a trajectory that the two photons interact with them. Each trajectory will be recorded in the sinogram (24).

The process of recording a LOR takes place after an annihilation event has occurred, and the two photons are recorded as a coincidence event. The photomultiplier tube (PMT) of each oppositely facing detector creates an electronic pulse from the luminescence created from the detected photon. First, the height of pulse should pass the low level of discriminator, then it needs to pass the timing window which a check by coincidence timing circuit (5-12 ns). After that, the energy window determines the level of acceptable energy detected from incoming photons. If the pulse passes these criteria, then a LOR is generated and recorded in a sinogram. This LOR can be from different coincidences. There are different types of coincidences, including true, random, and scatter coincidence. A true coincidence is defined when the two photons produced by a single nuclear transformation were detected simultaneously by two detectors (Figure 2(i)- A). A scatter coincidence is defined when either one or both photons produced by a single nuclear transformation are scattered and then both of them are detected (Figure 2(i)-C). A random coincidence is defined when different nuclear transformations are detected approximately simultaneously with the two detectors (Figure 1(i)-B) (24).

For each type of coincidence, a specific line of response (LOR) is recorded. While the LOR defines the pathway of detection of the two photons, there is still the problem of localizing the location of a nuclear transformation in the third dimension. Each LOR is recorded into a series of voxels, and it is known as a sinogram. An LOR is produced by two separate events that is detected

in opposite directions within the timing and energy window. If these events are recorded by two detector blocks in the same ring, this is called a direct-plain event. If these events are recorded by two adjacent blocks in the same ring, this is called a cross-plain event. PET images are reconstructed from the sinogram data, which contains LORs of direct- and cross-plain events. To localize the events of each LOR, instead of using Cartesian coordinates (x,y), polar coordinates are used for the LOR's location and are presented by (r,φ). The r term is the distance from the center and φ is the angle from the center. Based on the different types of coincidence events shown in Figure 2(i), the LORs recorded the information into the sinogram based on the angle and distance from the center (Figure 2 (ii)). These LORs are projected on to 2D histograms, then appears in a 3D volume, known as a voxel.

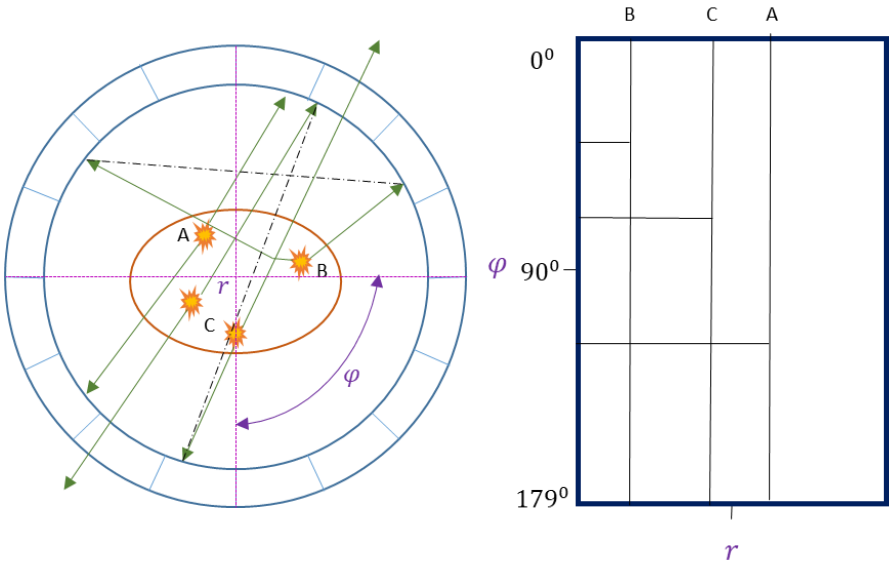

(i) (ii)

Figure 2. (i-A) A true coincidence is defined when the two photons produced by a single nuclear transformation were detected simultaneous by two detectors. (i-B) A scatter coincidence is defined when either one or both photons produced by a single nuclear transformation are scattered and then both of them are detected. (i-C) A random coincidence is defined when the different nuclear transformations occurred approximately simultaneously with two detectors. (ii) The LORs recorded with the information of angle and distance from the center, known as a sinogram.

3.1.2 Sensitivity

The number of counts (coincidence recorded) per second captured by the scanner from an activity in the field of view, is called the sensitivity (25). The sensitivity increases with the number of counts per unit of radiation dose and the length of the axial field of view of the scanner (AFOV). Recently, the available AFOV has increased from 20 up to 25 cm, leading to improved sensitivity by up to a factor of 40 (22). The sensitivity of PET scanners is usually between 1% to 2% (26). Normally, to increase the counts number, we could increase the scan time or we could increase the injected dose. The PET scanner with larger AFOV helps increase detection of gamma rays in both direct and cross plane directions since the gamma rays are emittedin isotropic directions, hence the detected number of counts per second is increased. However,with the increased AFOV we could reduce scan time or dose because we could record more counts. Therefore, the larger AFOV would have higher sensitivity. The GE Discovery MI PET/CT scanners with 3- and 5-ring detectors that are utilized in this study have an AFOV of 15 and 25 cm, respectively.

3.1.3 Radionuclide

A PET scan can image biochemical and physiological changes from a disease within the human body earlier than the anatomical imaging modalities such as computed tomography (CT) and magnetic resonance imaging (MRI). To indicate the physiological changes, PET scans require an appropriate radionuclide for the specific clinical indication. Each radionuclide has their own energy of beta emitter alongside positron range and half-life. The most common radionuclide in PET is fluorine-18-labeled with glucose called ^{18}F- fluorodeoxyglucose ($^{18}F - FDG$). The half-life is 109.75 minutes with a positron range of 2.4 mm (26). Some radionuclides are used to image

a dedicated function of an organ, including ^{18}F-sodium for brain imaging, Rubidium-82 for a myocardial perfusion, ^{18}F-fluciclovine for prostate cancer (27), ^{18}F-MISO [1H-1-3-[18F]fluoro-2-hydroxyproply] and ^{18}F-FAZA ([18F]fluoroazomycin arabinoside) for indicating the hypoxic area of tumor (28). In this study, the common radionuclide of $^{18}F-FDG$) was used.

Table 1 illustrates the various radionuclides used in PET scans for different clinical studies with their half-life and maximum positron energy value. Each positron emitter radionuclide has their own maximum energy. As the energy is increased the positron range is increased which means the radionuclide takes larger distance inside the body to deposit its energy and then interacts with the electron through the annihilation process to produce the two gamma rays in approximately opposite direction. As a result, the resolution in PET scan is dependent on the positron range and therefore on the radionuclide energy, the lower the range, the better the spatial resolution. Therefore, the difference between the location of accumulation of radionuclide and the location of annihilation process causes the degradation in PET imaging resolution.

Table 1. The various radionuclides were used in PET scan with their half-life and maximum energy value illustrates below. The common one is F18.

Nuclide	T1/2 (min)	Emax (MeV)
O15	2	1.72
N13	10	1.19
C11	20	0.96
F18	110	0.64

3.1.4 CT

A PET scanner is currently not available without a CT scanner as the advantages of the hybrid modalities are significant. The PET/CT scanner has a gantry for both modalities with a high-performance for each modality. The first part of the PET/CT scan is placing the patient on the table to obtain a CT scan and then the PET data acquisition is started. An advantage of using a CT scan is adding high resolution of anatomical information to physiological information of PET scan and converting CT image to the attenuation map that applied for attenuation correction of PET data. A great advantage of this hybrid modality is detecting disease and abnormal metabolic change inside the body with PET scan earlier than the anatomical change would be seen with a CT scan. It should be noted that the CT scan is acquired with a low dose protocol to decrease patient dose since it is used for creating an attenuation map, not for diagnosis.

3.2 Reconstruction Techniques of PET data

3.2.1 Iteration Reconstruction

The earliest PET scanners with one ring and the multi-ring detectors with septa, acquired the data in 2D and reconstructed with the 2-D Radon transform, called filtered back projection (FBP). Over time, since septa were removed to acquire the 3D PET data, the FBP technique was replaced by the statistically based reconstructed technique called iterative algorithms to improve the efficiency of image reconstruction and decrease image noise. The advantage of FBP when

compared to the iterative algorithms is the computation speed. However, the iterative algorithms are able to adopt a model to include the physics principle from the annihilation process to the coincidence detection and start from an assumption of an intrinsic statistics of radiation detection. The limitation of the image reconstitution accuracy is related to the approximation of the method and some intrinsic PET limitations, including the scatter coincidence and positron range.

The first iterative algorithm developed was the maximum-likelihood expectation maximization (ML-EM) (29) and is based on a Poisson model of the emission data (Figure 3). In this algorithm, an initial estimation of the reconstruction is assumed from the uniform image determined from the forward projection. The assumed image and the real image are compared to obtain a weighted matrix. This weighted matrix is used to update the reconstructed back projection estimate until the iterations converge.

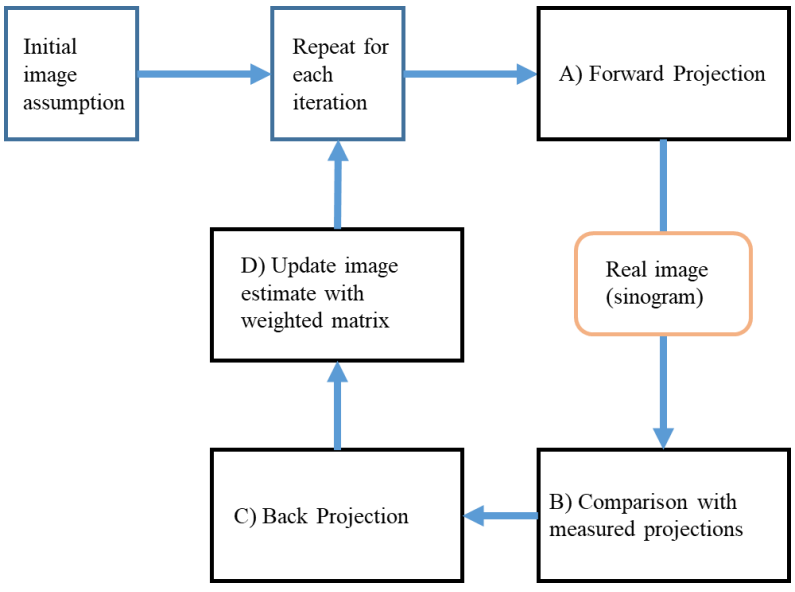

Figure 3. The flowchart diagram for MLEM iteration algorithm. This algorithm begins with an initial image assumption and then gets updates from the weighted matric that obtains from the comparison between the real image (sinogram) and the initial image assumption.

An advantage of the MLEM algorithm is maintaining of total counts in each iteration, ensuring a positive value for every voxel, and reaching convergence to the maximum likelihood estimate. A drawback of MLEM is the slow convergence that limits its clinical applications due to long computational times.

The more recent and common iterative algorithm is the ordered-subsets expectation maximization (OSEM) method to reconstruct the PET data more accurately. OSEM is a faster and more efficient reconstruction algorithm than MLEM. The OSEM reconstruction technique divides the PET data into ordered subsets that each have the same number of projections. The speed of iteration is increased as the PET data are divided into the various subsets, but also because one subset is used for each iteration. The drawback of this technique in comparison to MLEM is a lack of convergence to the maximum likelihood. With the same number of iterations for the MLEM and OSEM reconstruction techniques, the image quality is similar when the subsets are not high (30). The major advantage of OSEM is the faster iteration reconstruction technique, thus a feasible method to apply on PET data clinically. OSEM performed the quantitative results within 3% accuracy while the bias for lesion with the hotter background can increase up to 50%. A limitation of OSEM is that, to reach the full quantitative convergence, the effective iterations should increase, resulting in an increase in image noise.

One of the MLEM problems is the dependency of convergence on the initial data noise. Each iteration leads the reconstructed image being closer to convergence while it also causes increasing noise. The reason for this is related to Poisson random variables in the initial data sets. One solution is to determine the acceptance level of convergence and smoothness to stop the

iteration technique (31). The other solution is using the post-processing filter on the reconstruction after the acceptable level of convergence is met. This approach is beneficial since the acceptable level of image quality is determined with a post-processing cut-off frequency filter, and the acceptable level of noise is determined by the nuclear medicine physicians reading the images.

The other solution is using a smooth penalty factor in the likelihood distribution. In this approach, we need to have prior information to estimate the accepted smooth level of the image. Then with this information, the Bayesian estimation technique can be used with a regular iterative reconstruction technique (32) (Figure 4 and Equation 1).

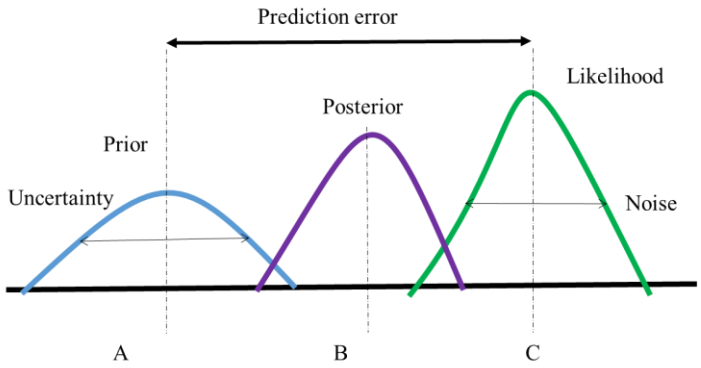

Figure 4. The schematic graph of Bayesian technique illustrates with a prior distribution (A), posterior distribution (B), and likelihood distribution (C). The prediction error is determined with the difference between the prior distribution and peak of likelihood distribution. The uncertainty is measured with the variance of the prior distribution and the noise is determined with the variance of the likelihood distribution.

Equation 1. $Posterior = Prior \times Likelihood$

Q. Clear is introduced by GE Healthcare as a reconstruction technique for PET/CT scanners that includes point spread function (PSF) modeling and controls noise level with determining a

penalty factor (β) (33). This technique implements higher smoothing in lower activity lesions and less smoothing in higher activity lesions. This results in the lower activity lesion being smoother and the hot lesion having a higher signal-to-noise ratio. This image reconstruction technique is implemented with the assumption of a Poisson model to maximize the penalized-likelihood objective function (17).

This technique provides an optimal tradeoff between image quality and quantification of PET data. This technique uses the relative difference penalty between the voxels to control noise and improve the resolution in an image. Advantages of this technique include better convergence, user inputs of the number of iteration and subsets, and determining the post-processing filter.

Figure 5 represents the pathway of reconstruction techniques of PET data for conventional and advance iterative reconstruction technique. The first three steps including dead time/normal correction, detector geometry modeling (LOR), and random correction are the same for both techniques. Forth step in Q. Clear, the point spread function is used which helpful to improve the activity in lesion and reduce the noise in image. Then, the scatter correction and ultralow dose computed tomography (UL-D CT) were applied on PET data in both reconstruction techniques. The last step of each reconstruction technique is different, the regularization for Q. Clear and the image filtering for conventional technique. The regularization is applied with the penalty function which is designed to improve the edges (spatial resolution) and reduce the background noise of image. Furthermore, the regularization provides a relationship between image quality and quantification in PET data.

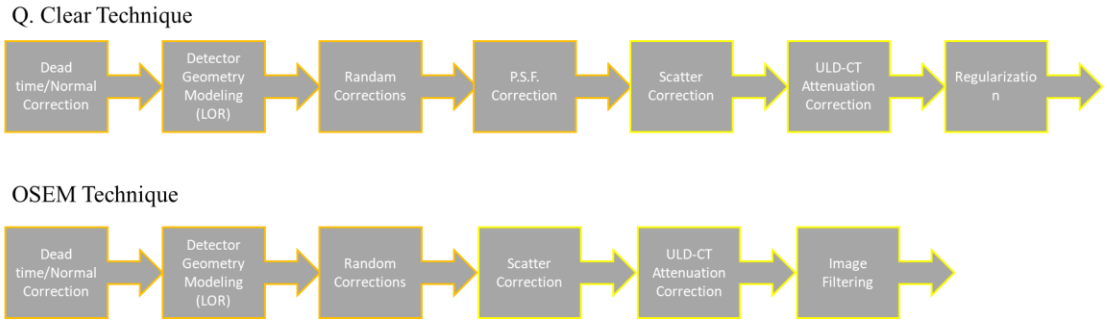

Figure 5. The reconstruction technique pathway represents in this diagram for the conventional iterative technique (OSEM) and the advance one (Q. Clear). The difference between these two techniques are the point spread function P.S.F) and regularization for Q. Clear and the image filtering for the conventional iterative reconstruction technique.

The Q. Clear algorithm is based on a Bayesian penalized likelihood (BPL) reconstruction technique which includes the additional term in the maximizing likelihood (conventional iterative algorithm). The conventional iterative algorithm illustrated in formula (Equation 2), where the y_i is the measurement PET coincidence data, x is an estimated image, and P is the system geometry matrix. In Q. Clear technique, the additional Beta term (Equation 3) increases alongside when noise increases, to reduce the objective function. This leads to optimize the reconstruction technique from a noisier image (19). Therefore, the full convergence will be achieved without the adverse effects of increasing noise found with conventional iterative (OSEM).

Equation 2. $$\hat{x} = arg\,max_{x\geq 0} \sum_{i=1}^{n_d} y_i\, log\big[Px\big]_i - \big[Px\big]_i$$

Equation 3. $$\hat{x} = arg\,max_{x\geq 0} \sum_{i=1}^{n_d} y_i\, log\big[Px\big]_i - \big[Px\big]_i - \beta R(x)$$

The R(x) term is defined as a penalty to control noise and the β term is called a penalization factor which controls the relative strength of the regularizing term with respect to the data statistics (19). The relative difference penalty technique (RDP) is used in Q. Clear reconstruction algorithm which is helpful to provide activity dependence on noise control. The RDP formula (Equation 4) is defined as including the relative weights (w_j and w_k) for different components of the function and γ is a tunable parameter to control the edge preservation.

Equation 4. $$R(x) = \sum_{j=1}^{n_y} \sum_{k \in N_j} w_j w_k \frac{(x_j - x_k)^2}{(x_j + x_k) + \gamma |x_j - x_k|}$$

The block sequential regularized expectation maximization (BSREM) technique is used in Q. Clear to solve the equation 3 (18, 34). By using BSREM technique, each image voxel will achieve full convergence (100%) in comparison to the OSEM algorithm that will achieve partial convergence. By using the regularization modulation, the optimal tradeoff between the image quality and quantification evaluation would be determined. The other advantage of Q. Clear is that the user needs to determine the penalization factor (β) that will preserve the edge and reduce the background noise image while in the OSEM technique the user required to determine the number of iteration, subset, and the post-filter (Gaussian filter).

In our clinic, the patient's PET image data is reconstructed with a 3D maximum likelihood ordered subset expectation maximization (3D OSEM) and time-of-flight (TOF) technique with 2.5 min/bp, 4 iterations, 16 subsets, and a 5 mm post-processing (Gaussian) filter. This setup was optimized on the Discovery MI PET/CT with a 3-ring scanner by a Nuclear Medicine technologist

of the hospital, and it defined the Clinical OSEM (C. OSEM) reconstruction technique used on the phantom scans for this study. This same reconstruction protocol is also implemented on our institution's 5-ring Discovery MI PET/CT scanner. These two scanners are equipped with GE's BPL reconstruction algorithm known as the Q. Clear technique. As discussed previously, Q. Clear could be defined as an OSEM. TOF, PSF, BPL with a noise suppression factor of β (33). The one user-defined parameter is the β value and there is not one optimal β penalization value. This value depends on various elements including the type of radiopharmaceutical, the amount of activity, the scan time (min/bp), the PET scanner model, and the image reconstruction technique (35). As the recommended value of β is 350, the phantom study was designed for the value of 300 – 600 with steps of 100 and 1000 to simulate the wide range of β values and evaluate the effect on the quantitative image quality parameters.

3.3 Image Quality parameters

3.3.1 Contrast Recovery (CR)

The average counts in each hot sphere (10, 13, 17, and 22 mm diameters) ($C_{H,j}$) were measured and each cold sphere of the NEMA IQ phantom (28 and 37 mm) ($C_{C,j}$) were measured. The average of the background ROI counts for the sphere is equal to $C_{background,j}$. The radioactivity concentration in the hot spheres (a_H) and the concentration of radioactivity in the background ($a_{background}$) is calculated. The contrast recovery (CR_j) for the hot and cold spheres are defined in equation 1 and 2, respectively (36-38) (Equation 6 and 7).

Equation 5. $CR_{H,j} = \frac{\left(\frac{C_{H,j}}{C_{background,j}}\right)-1}{\left(\frac{a_H}{a_{background}}\right)-1} \times 100\%$

Equation 6. $CR_{C,j} = \left(1 - \frac{C_{C,j}}{C_{background,j}}\right) \times 100\%$

3.3.2 Background variation (BV)

The standard deviation is defined by equation (3) where *k* is the number of background ROIs and the $C_{background,j,k}$ is the average counts of the background ROI for the specific sphere. The percent background variability (%BV) for each sphere *j* is calculated by the ratio of the standard deviation (SD) over the average counts in the background (36-38)(Equations 8 and 9).

Equation 7. $SD_j = \sqrt{\frac{\sum_{k=1}^{k=60}\left(C_{background,j,k} - C_{background,j}\right)^2}{k-1}}$

Equation 8. $BV_j = \frac{SD_j}{C_{background,j}} \times 100\%$

3.3.3 Contrast-to-noise ratio (CNR)

The other image quality parameter analyzed in this study is the contrast-to-noise ratio (CNR). The CNR was calculated using equation 6 where the CR of each hot and cold lesion was divided by the respective BV value of that sphere (38) (Equation 10).

Equation 9. $CNR_j = \frac{CR_j}{BV_j}$

3.3.4 Lung Residual Error (LRE)

As the LRE is defined by equation 7, this parameter is used to evaluate the accuracy and scatter correction in the lung insert of the NEMA phantom (37, 38). The average counts in the lung insert of the NEMA phantom is $C_{lung,i}$ (9) (Equation 11).

Equation 10. $LER_i = \frac{C_{lung,i}}{C_{B,i}} \times 100\%$

3.4 Literature Review

The β values of the Q. Clear reconstruction technique for this study were determined from previous studies. Teoh et al (33) used the NEMA phantom study to evaluate the optimum penalization factor (β) with a range of 100-1000 with ^{18}F-FDG. Their IQ quality parameters evaluation included the CR and BV on the phantom study and their patient data was evaluated by two radiologists scorers based on the overall IQ, background liver, mediastinum and marrow IQ, noise level, and lesion detectability of fifteen oncology patient with whole body ^{18}F-FDG PET scan. They recommended a β value of 400 using the Q. Clear reconstruction technique.

The Teoh et al (27) study performed the Q. Clear reconstruction technique with a β range of 100-600 for recurrent prostate cancer imaging with ^{18}F-Fluciclovine. The patient study assessment parameters included standard uptake value (SUV_{max}), organ SUV_{mean}, and the standard deviation and was evaluated by two radiologist readers with scoring the overall IQ, noise level, background marrow IQ, and lesion conspicuity. This study suggested a β value of 300 for this particular radiotracer for recurrent prostate cancer.

Reynes-Llompartet al (39) performed the Q. Clear reconstruction technique with a β range of 50-500, at intervals of 50 for both phantom and patients study. IQ parameters were evaluated by using contrast-to-noise ratio (CNR) and background variability for phantom. Fifteen ^{18}F-FDG oncology patients (ten torso and five brain scans) were reconstructed with the Q. Clear reconstruction technique and the noise, contrast, and signal-to-noise ratio (SNR) were computed for each lesion. Two different nuclear medicine physicians assessed the IQ of PET data. The phantom and patient study recommended a β value of 350 for ^{18}F-FDG oncology scans and a β value of 200 for a brain PET/CT scan based on their CNR assessment of the phantom and SNR evaluation of patients.

Rogasch et al (15) performed the Q. Clear reconstructed technique with various β values of 150, 300, and 450 on the NEMA phantom with various scan time on Discovery MI PET/CT with 3-ring detector. The IQ parameters of spatial resolution from 3D sphere activity profile, CR, and SNR were evaluated. They recommended values of β of 300 and 450 based on the tradeoff between the CR and SNR with the Q. Clear with β values of 300 and 450. However, a validation for a patient with various activity and acquisition protocols may have been needed.

Wyrzykowski et al (40) performed the Q. Clear reconstruction technique with the GE default β value of 350 to determine the effect of reconstruction techniques on SUV_{max} values. The images of a total of 280 ^{18}F-FDG oncology patients' with lymphoma were reconstructed with their standard OSEM and Q. Clear technique with penalization factor of 350. Their evaluations were classified based on the purpose of the images including for staging (sPET), early treatment response (iPET), and the end of treatment (ePET). They recommended using standard OSEM for the treatment respond PET images might be more accurate while the Q. Clear may change the

interpretation of small lesions. Therefore, based on the different studies, the range of β values used in this study was 300, 400, 500,600, and 1000.

4. Methods

4.1 PET/CT scanners

There are two GE Health Discovery MI PET/CT systems installed at Oregon Health and Science University (OHSU). One of the PET Units has 3-rings of detectors with the PET scanning field of view (FOV) of 15 cm, and the other one has 5-rings of detectors with a FOV of 25 cm. The 5-ring PET/CT Discovery MI (25 cm FOV) is located on the 4th floor of Peter O. Kohler Pavilion in the Radiation Medicine Department of the University Hospital on OHSU's main campus. The 3-ring PET/CT Discovery MI (15 cm FOV) is located at OHSU's Knight Cancer Institute clinic in Beaverton, OR. Both units are capable of reconstructing PET data with 3D ordered subset expectation maximization (OSEM), Time-of-Flight (TOF), point-spread function (PSF), and Q. Clear with a wide range of β-value. The Computed Tomography (CT) aspect of both systems is the GE Revolution and has a 64-slice detector, 50 cm FOV, and uses attenuation correction of PET data to improve the anatomical information.

4.2 NEMA Image Quality Phantom

The National Electrical Manufacturers Association (NEMA) body image quality phantom (37) has a dimension of 24 × 30 × 24 cm^3 that contains six spheres with the same distance from the center of the phantom. The sphere diameters are 10, 13, 17, and 22 mm to simulate hot lesions that will contain the radioactive solution, and 28 and 37 mm diameter spheres to simulate cold lesions that will only contain water. At the center of the phantom, there is a cylindrical insert 5 cm in

diameter to represent a lung with a density of 0.30 $\frac{g}{cm^3}$ (36). A solution of $^{18}F-FDG$ in water was used to simulate the ratio of 4:1 radioactivity concentration in the hot lesions vs. background.

The phantom was prepared and scanned with suggested protocols according to the instructions in the GE Healthcare, DISCOVERY MI, NEMA (25) Test Procedures and Detector Performance Test document (41). First, the phantom was filled to one-fourth of its total volume (2448 ml, total volume equal to 9792 ml) with water (Figure 6). The activity of FDG was measured by a dose calibrator to identify the amount of activity and the required volume of FDG to fill the phantom. The required volume activity was measured by syringe, and then the time and amount of activity was recorded. These numbers were imported into the scan protocol to calculate the amount of activity at the time of scan. The recommended activity of the background and hot spheres according to the NEMA protocol tests was 5.3 kBq/cc (0.15 μCi/cc) and 21 kBq/cc (0.6 μCi/cc), respectively at the scan time. The measured activity was added to water already in the phantom and mixed well to provide a uniform activity concentration. Second, 20 ml of this mixture was used to fill the four hot spheres (10, 13, 17, and 22 mm) to provide a concentration of 4:1 ratio to the background. A syringe was used to fill the four hot lesions with the activity solution, and the two other spheres (28 and 37 mm) were filled with water to represent cold lesions with no activity. Lastly, the remaining empty ¾ of the phantom was filled with water and placed on the scanner's table (Figure 7). The phantom's background activity and concentration were nearly identical for the phantom scans on each PET unit. The background activity of phantom on each scanner was 4.6 and 4.7 kBq/cc (0.12 and 0.13 μCi/cc) for the 3- and 5-ring scanner, respectively.

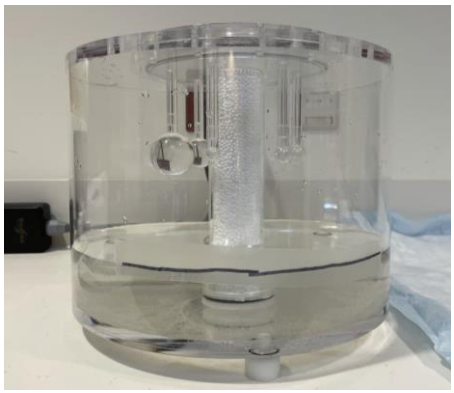

Figure 6. The NEMA Image Quality phantom was initially filled with water to 25% of its total volume and then the measure FDG activity was added to that by syringe.

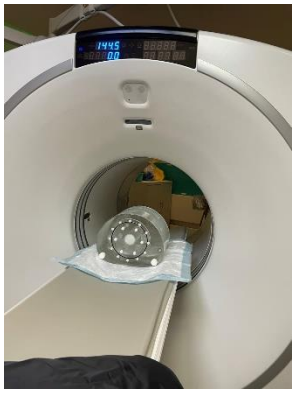

Figure 7. The prepared NEMA phantom was put on the table of the Discovery MI (25 cm FOV) in preparation for the scan

4.3 Data acquisition

The phantom was placed on the scanner's table and centered it in the sagittal and coronal planes by aligning the laser light the center of the phantom. The orientation of the phantom on the table should present the smallest sphere at 1 o' clock in the coronal plane of the phantom. The process of data acquisition was started by selecting the NEMA Image Quality protocol on the GE scanner that provided preset CT and PET scan parameters. The CT scan of the NEMA phantom was completed using the GE NEMA Image Quality protocol, which was corresponded to a helical head

protocol, with techniques of: 0.5 second rotation times, tube potential of 140 kV, tube current set to Auto, 3.75 mm slice thickness, pitch of 0.984, PET AC reconstruction technique, and field of view 70 cm. The PET scan of the phantom was performed with a scan time of 6 minutes with starting background activity of 4.6 and 4.7 kBq/ml on the 3- and 5-rings PET/CT systems, respectively. The initial PET images were reconstructed with the VPFX (3D OSEM) reconstruction technique, using CTAC as attenuation correction, 40 cm reconstruction FOV, four iterations, 34 subsets, and a 2 mm Gaussian filter (37). The phantom image data was reconstructed with other reconstruction techniques, including our clinical OSEM (C. 3D OSEM+TOF) (with 16 iterations and 5 mm Gaussian filter instead) and the Q. Clear technique with a range of the β-values (300, 400, 500, 600, and 1000). These reconstructions were applied to both the 3- and 5-ring scanner's image data.

As the aim of this study was to investigate the possibility of decreasing the scan time from the current clinical standard, the phantom image data were simulated with scan times from 1 – 4 minute at 30 second intervals, and 4 - 6 minutes with 1 minute intervals. The scan times of 1, 1.5, and 2 minutes were selected to simulate 40%, 60%, and 80% of the standard scan time. These scan times were implemented for each reconstruction simulation on the C. OSEM and Q –clear with the varying β-values reconstruction techniques. The current clinical standard reconstruction technique is the C. OSEM reconstruction technique with a scan time of 2.5 min/bp. All other image quality data were compared to this technique on both scanners.

4.5 Image Quality Analysis

The Image Quality (IQ) data was collected using the GE NEMA PET analysis tool (GE healthcare) available on each GE PET/CT. Before we could run the analysis tool, the hot spheres activity concentration ratio to that of the background was entered. For our study the ratio was entered as "4:1" as the activity concentration of the hot spheres was 4 times that of the background. When the specific reconstructed PET image data set was selected, and the contrast ratio was typed into the GE IQ tool, the IQ report of the specific image data would be available after a few minutes. Figure 8 shows the IQ report of the PET data on a 5-rings scanner with Q. Clear reconstruction technique (β-value= 400), and 2.5-minute scan time

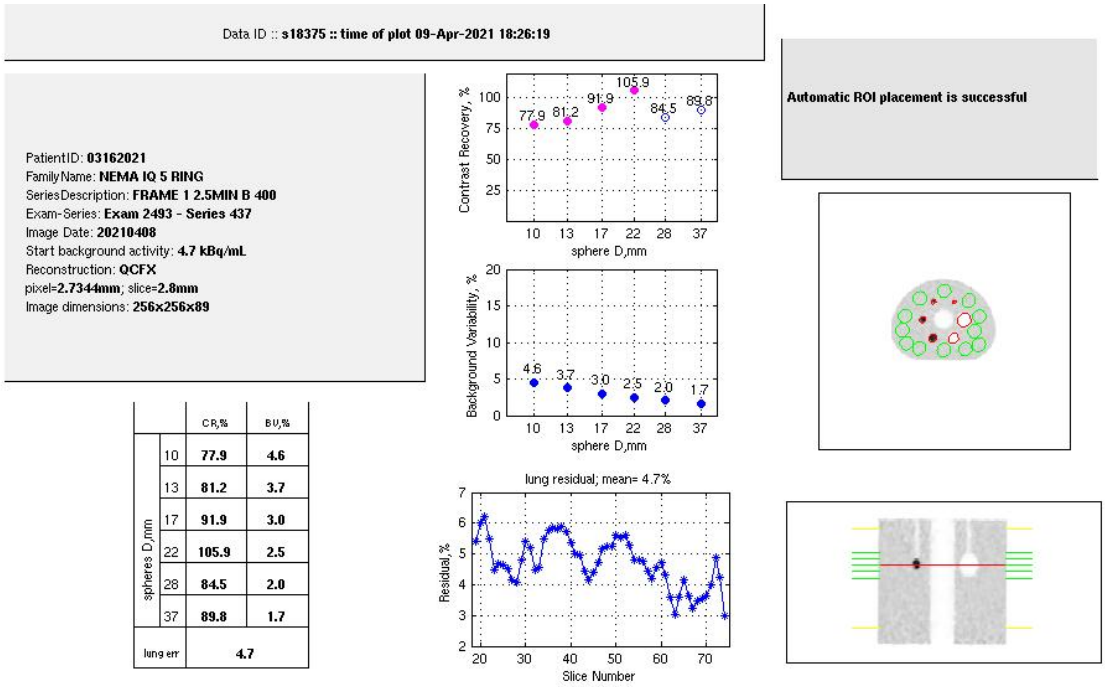

Figure 8. The report of Image Quality evaluation for the PET image data of NEMA phantom that was reconstructed with the Q. Clear technique, β value of 400, and scan time of 2.5 minutes. The Image Quality parameters given include the percent Contrast Recovery of both hot and cold spheres), the percent Background variability (%BV), and the percent Lung Residual Error (%LRE). On the right side, the position of the region of interest (ROI) at both axial and coronal views is illustrated.

For convenience, the phantom image data from both scanners were placed on the Discovery MI PET/CT with 5-rings and the image quality section on the PET analysis tool was used to obtain the various IQ parameters. Next, Image Quality tool was run and the software automatically drew circular ROIs with the same diameter of each sphere on the CT images of the phantom as well as the ROIs on the PET data. In the background area of the phantom, twelves ROIs of 37 mm in diameter were drawn in the central image and in the images at ± 10 mm and at ± 20 mm from the central image. The ROI of each sphere (10, 13, 17, 22, 28, and 37 mm) was drawn appropriately concentric to the twelves background ROIs with 37 mm diameter size at the middle image. Finally, a circular ROI with a 3 cm diameter size and a same length of the phantom was drawn in every image of the phantom in the central cylindrical lung insert (36). An example of the ROIs automatically drawn by the system is shown in Figure 7. The GE Image Quality tool was run for each combination of scan times and reconstruction techniques mentioned previously. Screenshots of each IQ report as seen in figure 7 were saved so the individual IQ parameters could be recorded and analyzed.

The values of IQ parameters, including CR, BV, and LRE were manually imported into Excel to compare these parameters. The CNR was calculated for each data set by dividing each CR value over its corresponding BV value. The baseline value for each image quality parameters was established using the current routine clinical reconstruction technique (C. OSEM) with 2.5 min scan time on the 3-ring scanner. These baseline IQ parameter values were then compared with the IQ parameters values of the other data sets. Comparing the CR, BV, LRE, and CNR values of each reconstruction technique and scan time to the baseline values allowed analysis of the effect of the reconstruction and scan time on the above IQ parameters. A line graph was created for the CR, CNR, and BV values to evaluate the trend of the hot and cold spheres on each reconstruction

technique while the scan time was varied. This comparison was applied to find if any combination of scan time and reconstruction technique would provide better or the same image quality as our clinical standard. Specifically, an increase in the CR value, decrease in the BV value, or increase in CNR would give evidence of improving image quality.

5. Results

The NEMA Image Quality phantom data for both the 3 and 5 ring PET systems were analyzed as part of this study. The CR, BV, and Lung residual errors were measured for each PET system at each reconstruction technique with the IQ assessment tool of the GE system. In addition to these IQ parameters, the CNR values were calculated and analyzed. The results of these IQ parameters present in Tables 2 through 7 and Figures 9 through 15.

5.1 Contrast Recovery (CR)

Table 2 represents the contrast recovery data of the NEMA IQ phantom scanned with the GE Discovery MI PET/CT with a 3-ring detector and reconstructed with various reconstruction techniques and scan times. From Table 1, the CR values for all sphere sizes were reduced with an increasing β-value of the Q. Clear reconstruction technique. Increasing scan time for each reconstruction technique led to a decrease in the CR values for the smallest hot spheres and no change in the CR for the cold spheres. Among the hot spheres, the largest one has the highest CR compared to all other spheres. The CR of the clinical OSEM (C. OSEM) reconstruction technique at the current clinical standard of 2.5 minute scan time was lower than the CR with β-values less than 600 and OSEM reconstruction technique recommended by GE for NEMA testing (OSEM)for every scan time. However, the 2.5 minute C. OSEM CR value was higher than the CR for the β-values 600 and 1000 for every scan time in the hot and cold spheres. Figure 9-A and 9-B represent the contrast recovery data of both hot and cold spheres of the NEMA phantom scanned on the GE PET/CT scanner with 3-ring detector and reconstructed with Q. Clear reconstruction technique (β

= 300 and 1000), respectively. Figure 9-C presents the contrast recovery values of the clinical standard reconstruction technique for varying scan times.

Table 2. The NEMA IQ phantom contrast recovery (CR) data for the 3-ring PET/CT scanner for hot sphere (10, 13, 17, and 22 mm) and cold sphere (28 and 37 mm) at various scan time (1-6 minutes). The standard reconstruction of the clinic is presented by the bold line around the row. Green shade cells indicate the higher CR of technique with the same or lower scan time than the standard reconstruction.

Reconstruction Technique	Sphere (mm) / Time	10	13	17	22	28	37
B 300	1 min	72.4	72.0	59.2	83.8	79.6	85.6
	1.5 min	57.0	69.2	61.0	80.6	82.3	85.2
	2 min	54.9	67.2	60.5	79.0	83.7	85.9
	2.5 min	53.4	66.1	64.7	80.7	83.1	85.2
	3 min	50.4	68.9	63.5	79.6	83.3	84.9
	3.5 min	48.8	68.3	65.0	80.1	83.1	84.9
	4 min	47.6	66.0	67.6	81.5	83.6	85.1
	5 min	50.4	62.3	68.5	81.4	82.5	85.2
	6 min	52.3	64.1	72.0	82.5	82.8	85.3
B 400	1 min	64.4	68.2	59.8	82.4	70.3	84.8
	1.5 min	51.7	65.9	61.2	79.3	80.9	84.2
	2 min	49.2	64.2	60.5	78.1	82.0	84.9
	2.5 min	47.8	63.1	64.3	79.7	81.5	84.2
	3 min	45.0	65.7	63.6	78.8	81.7	83.9
	3.5 min	43.5	65.1	64.5	79.3	81.5	83.9
	4 min	42.6	63.3	66.7	80.8	81.9	84.2
	5 min	45.2	60.0	67.8	80.5	81.1	84.2
	6 min	47.2	61.7	71.2	81.7	81.1	84.3
B 500	1 min	57.8	64.5	59.8	81.4	77.1	84.1
	1.5 min	46.4	62.8	61.6	78.3	79.4	83.4
	2 min	44.3	61.4	60.2	77.4	80.5	84.0
	2.5 min	43.2	60.3	63.7	79.0	80.0	83.2
	3 min	40.6	62.7	63.0	77.9	80.2	83.0
	3.5 min	39.0	62.4	63.8	78.6	79.9	83.0
	4 min	38.2	60.6	65.8	79.9	80.3	83.2
	5 min	40.5	57.6	66.8	79.7	79.5	83.2
	6 min	43.1	59.4	70.5	80.8	79.7	83.2
B 600	1 min	52.4	61.3	59.6	80.4	76.0	83.2
	1.5 min	42.3	59.9	61.2	77.4	78.1	82.5
	2 min	40.3	58.6	59.7	76.7	79.1	83.1
	2.5 min	39.3	57.6	62.9	78.2	78.6	82.4

Reconstruction Technique	Sphere (mm) / Time	10	13	17	22	28	37
	3 min	37.0	59.9	62.3	77.2	78.8	82.2
	3.5 min	35.9	59.7	63.0	77.9	78.6	82.2
	4 min	34.8	58.1	64.8	79.1	78.9	82.4
	5 min	37.1	55.1	65.8	78.9	78.1	82.4
	6 min	39.8	57.3	69.6	79.8	78.3	82.4
B 1000	1 min	38.3	50.9	57.4	76.9	72.0	80.5
	1.5 min	31.2	50.5	58.4	74.3	73.7	79.6
	2 min	29.7	49.4	56.4	74.0	74.5	80.1
	2.5 min	29.1	48.6	59.2	75.1	74.1	79.4
	3 min	27.6	50.5	58.5	74.2	74.0	79.2
	3.5 min	26.6	50.5	59.2	75.1	73.8	79.2
	4 min	25.7	49.4	60.6	76.2	74.2	79.4
	5 min	27.1	47.2	61.6	76.0	73.5	79.4
	6 min	30.6	49.8	65.7	77.1	74.2	79.4
OSEM	1 min	80.5	69.4	54.2	84.8	80.0	84.8
	1.5 min	65.0	68.3	57.6	83.7	84.9	85.2
	2 min	60.5	65.3	56.2	81.4	88.2	86.9
	2.5 min	60.5	64.0	62.8	83.8	87.6	86.5
	3 min	58.7	68.1	60.7	82.0	87.3	86.1
	3.5 min	56.4	67.7	61.9	82.1	87.4	86.4
	4 min	58.1	64.2	65.6	83.3	87.7	86.9
	5 min	58.6	59.9	66.8	82.4	86.6	87.6
	6 min	58.7	60.4	69.5	82.9	86.3	87.6
C. OSEM	1 min	55.2	62.9	57.2	75.3	73.3	81.2
	1.5 min	49.1	58.4	58.3	75.7	75.9	80.8
	2 min	49.8	57.0	59.9	75.3	77.5	81.4
	2.5 min	49.1	57.5	61.8	75.6	77.3	80.7
	3 min	46.2	57.9	61.3	74.0	77.7	80.7
	3.5 min	45.6	58.5	61.5	75.0	77.7	80.9
	4 min	45.4	56.9	63.3	75.7	77.9	80.9
	5 min	48.8	55.1	64.4	75.9	77.3	81.1
	6 min	50.2	56.0	66.8	76.3	77.7	81.3

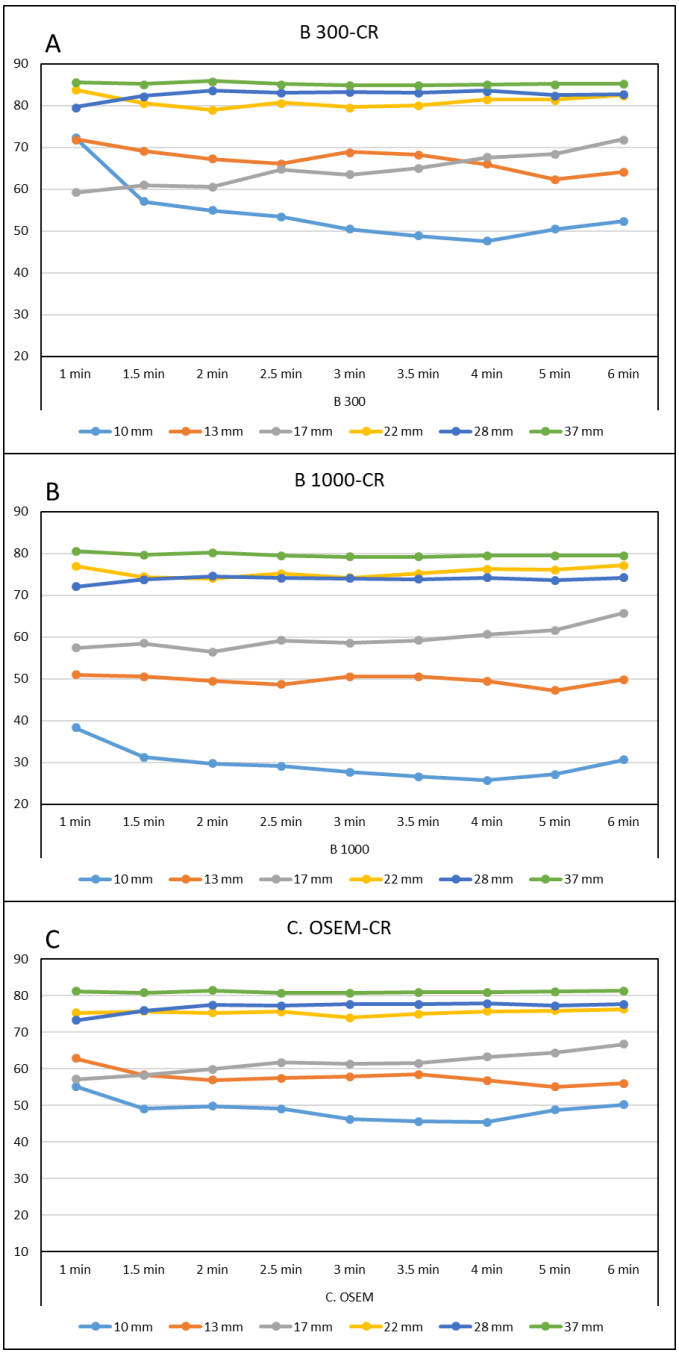

Figure 9. The NEMA IQ phantom CR values for Q. Clear (β = 300 and 1000) and standard reconstruction at various scan times for its different spheres' sizes on the 3 ring PET system. A- PET data reconstructed with Q. Clear with β= 300; B- PET data reconstructed with Q. Clear with β= 1000; C- PET data reconstructed with standard reconstruction technique (OSEM+TOF).

Similarly, to Table 2, Table 3 represents the contrast recovery data of the NEMA phantom that was scanned on the GE Discovery MI PET/CT with a 5-ring detector and reconstructed with

various reconstruction techniques and scan times. As shown in Table 2, the CR values for all spheres were reduced with an increase of the β-value of the Q. Clear reconstruction technique. Increasing scan time for each reconstruction technique leads to an increase in the CR for the second smallest hot spheres (13 mm) and no change in the CR for the cold spheres. Again, the largest hot sphere has the highest CR value of all spheres. The CR of the C. OSEM reconstruction technique with the 2.5 minute scan time was lower than the CR of Q. Clear withβ-values less than 1000 and OSEM for every scan time at both hot and cold spheres, but it was higher than the CR for the β-value of 1000 at both hot and cold spheres for every scan time. Figure 10-A and 10-B represent the contrast recovery data of both the hot and cold spheres of the NEMA phantom scanned with the GE PET/CT scanner with a 5-ring detector and reconstructed with Q. Clear reconstruction technique (β = 300 and 1000), respectively. Figure 10-C presents the contrast recovery value of the current clinical standard reconstruction technique for varying scan times.

Table 3. The NEMA IQ phantom contrast recovery (CR) data for the 5-ring PET/CT scanner for hot sphere (10, 13, 17, and 22 mm) and cold sphere (28 and 37 mm) at various scan time (1-6 minutes). The standard reconstruction of the clinic is presented by the bold line around the row. Green shade cells indicate the higher CR in compare to the standard reconstruction technique.

Reconstruction Technique	Spheres (mm) / Time	10	13	17	22	28	37
B 300	1 min	82.2	84.3	93.1	108.0	83.9	90.8
	1.5 min	89.0	85.1	92.1	106.5	85.4	90.8
	2 min	86.1	85.7	94.8	109.6	84.9	90.9
	2.5 min	85.0	86.2	95.2	109.2	85.9	90.7
	3 min	87.1	88.7	94.4	108.8	86.1	90.6
	3.5 min	85.3	89.8	96.4	109.3	87.1	90.3
	4 min	84.0	90.2	96.1	107.9	86.9	90.3
	5 min	84.7	92.5	97.2	107.8	87.0	90.1
B 400	1 min	75.7	79.3	90.0	104.6	82.6	89.7
	1.5 min	81.7	80.4	89.3	103.0	83.9	89.7
	2 min	79.1	80.7	91.8	105.9	83.6	90.1
	2.5 min	77.9	81.2	91.9	105.9	84.5	89.8
	3 min	79.9	83.6	91.2	105.2	84.3	89.3

Reconstruction Technique	Spheres (mm) / Time	10	13	17	22	28	37
	3.5 min	78.4	84.7	92.7	105.8	85.5	89.1
	4 min	77.1	85.0	92.8	104.6	85.1	89.1
	5 min	78.0	87.1	93.5	104.7	85.2	88.9
	6 min	79.8	91.1	95.1	106.5	85.3	89.1
B 500	1 min	71.6	77.6	89.0	103.8	81.8	89.0
	1.5 min	77.1	78.3	88.6	102.2	82.9	89.0
	2 min	75.1	78.5	91.0	104.9	82.5	89.3
	2.5 min	73.6	78.9	90.9	104.5	83.4	89.0
	3 min	75.5	81.0	90.0	104.1	83.2	88.6
	3.5 min	74.0	81.9	91.4	104.6	84.3	88.4
	4 min	73.0	82.4	91.5	103.6	83.9	88.4
	5 min	73.1	84.2	92.1	103.9	84.0	88.1
	6 min	75.1	88.2	93.9	105.6	84.1	88.3
B 600	1 min	67.6	75.7	87.9	102.9	80.9	88.3
	1.5 min	72.8	76.2	87.8	101.4	81.9	88.3
	2 min	71.1	76.4	90.1	103.9	81.5	88.6
	2.5 min	69.7	76.5	89.8	103.7	82.2	88.3
	3 min	71.4	78.7	88.9	103.2	82.1	87.9
	3.5 min	70.0	79.5	90.3	103.6	83.2	87.7
	4 min	69.2	79.9	90.3	102.6	82.9	87.6
	5 min	68.9	81.5	90.8	103.7	83.1	87.4
	6 min	71.1	85.5	92.6	104.8	83.1	87.6
B 1000	1 min	53.8	69.0	83.8	99.6	77.8	85.7
	1.5 min	58.4	68.6	84.1	98.4	78.3	85.7
	2 min	57.8	68.4	86.1	100.4	77.9	86.0
	2.5 min	56.1	68.6	85.6	99.9	78.6	85.6
	3 min	57.6	70.2	84.5	100.0	78.4	85.3
	3.5 min	56.4	70.6	85.7	100.0	79.3	85.0
	4 min	55.9	71.0	85.6	99.2	78.8	84.9
	5 min	54.8	72.4	86.0	99.3	79.2	84.7
	6 min	58.2	76.5	88.2	101.6	79.5	85.1
OSEM	1 min	71.6	75.9	92.2	106.2	83.1	90.4
	1.5 min	82.0	79.4	89.3	103.8	86.9	91.4
	2 min	80.9	78.9	91.4	106.7	87.0	92.2
	2.5 min	78.4	79.5	92.0	107.8	88.7	92.1
	3 min	80.0	81.7	91.3	106.4	88.8	91.6
	3.5 min	78.1	84.6	93.3	107.6	90.4	91.6
	4 min	77.4	85.4	93.6	105.5	90.3	91.6

Reconstruction Technique	Spheres (mm) / Time	10	13	17	22	28	37
	5 min	80.2	88.8	95.3	106.2	90.0	91.7
	6 min	80.8	89.6	93.5	105.9	89.8	91.5
C. OSEM	1 min	62.0	69.6	79.2	98.9	77.0	84.3
	1.5 min	68.5	71.5	77.4	97.9	78.4	84.7
	2 min	67.3	70.0	79.6	101.2	77.7	85.1
	2.5 min	66.7	70.9	80.1	99.8	78.5	84.6
	3 min	68.9	72.5	80.2	99.2	78.3	84.3
	3.5 min	77.6	80.6	82.7	101.7	79.8	84.0
	4 min	66.5	74.6	80.9	98.2	79.1	84.0
	5 min	67.6	76.6	82.1	98.8	79.1	83.7
	6 min	80.8	89.6	93.5	105.9	89.8	91.5

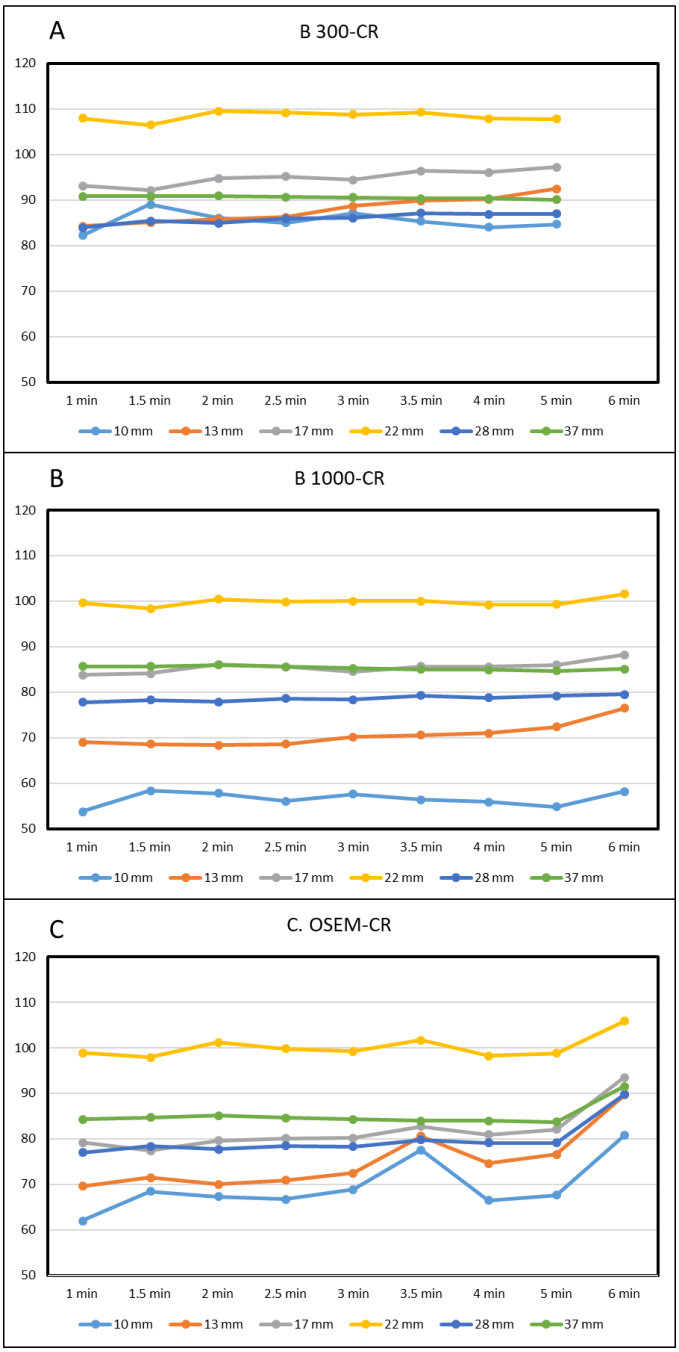

Figure 10. The NEMA IQ phantom CR values for Q. Clear (β = 300 and 1000) and standard reconstruction at various scan times for its different spheres' sizes on the 5 ring PET system. A- PET data reconstructed with Q. Clear with β= 300; B- PET data reconstructed with Q. Clear with β= 1000; C- PET data reconstructed with standard reconstruction technique (OSEM+TOF).

On average, the 5-ring CR values with Q. Clear reconstruction technique with every β value at various scan times is almost 1.4 higher than the 3-ring CR value with C. OSEM and 2.5 minute' scan time for the hot spheres. The CR values were fairly similar for the cold spheres on both systems. When comparing the 3-ring with C. OSEM at 2.5 minutes and the 5-ring with C. OSEM for different scan times, the average CR value of the 5-ring scanner at every scan times was 1.3 times higher the 3-ring scanner at 2.5 minute scan time for all hot spheres while the CR values were the same for the cold spheres at both systems at every scan time.

5.2 Background Variation (BV)

Table 4 represents the background variation data of the NEMA phantom that was scanned with the GE Discovery MI PET/CT with a 3-ring detector and reconstructed with various reconstruction techniques and scan time. The BV for all spheres decreased as the β-value of the Q. Clear reconstruction techniques was increased. Increasing the scan time for each reconstruction technique led to a decrease in the BV for both hot and cold spheres. The 10 mm hot sphere had the highest BV compared to the other hot spheres at any scan time for each reconstruction technique. The C. OSEM reconstruction technique has lower BV than the OSEM for every scan time and both hot and cold spheres. The BV of the C. OSEM reconstruction technique at the current clinical standard scan time of 2.5 was lower than the BV of the Q. Clear reconstruction technique with the following reconstruction parameters: β-value of 300 and 400 with scan times of 1 through 2 minutes, β-value of 500 and 600 with scan times of 1 and 1.5 minutes, and β-value of 1000 at scan time of 1 minute. The BV values for the 2.5 minute C. OSEM reconstruction technique was higher than the BV of all the other β-values for every scan time in all spheres. Figures 11-A and 11-B

represent the background variation data of both hot and cold spheres of the NEMA phantom scanned with the GE PET/CT scanner with a 3-ring detector and reconstructed with Q. Clear reconstruction technique (β = 300 and 1000), respectively. Figure 11-C presents the background variation values of the clinical standard reconstruction technique.

Table 4. The NEMA IQ phantom background variation (BV) data for the 3-ring PET/CT scanner for hot sphere (10, 13, 17, and 22 mm) and cold sphere (28 and 37 mm) at various scan time (1-6 minutes). The standard reconstruction of the clinic is presented by the bold line around the row. Green shade cells indicate the higher BV value with the same or lower scan time in compare to the standard reconstruction technique.

Reconstruction Technique	Spheres (mm) / Time	10	13	17	22	28	37
B 300	1 min	10.4	8.9	7.3	5.9	4.6	3.7
	1.5 min	9.0	7.6	6.3	5.2	4.3	3.3
	2 min	7.5	6.6	5.7	4.9	3.9	2.9
	2.5 min	6.7	5.8	4.8	4.0	3.1	2.4
	3 min	6.3	5.5	4.6	3.8	3.0	2.3
	3.5 min	5.9	5.1	4.3	3.6	2.8	2.2
	4 min	5.2	4.6	4.0	3.4	2.7	2.0
	5 min	5.1	4.5	3.8	3.1	2.4	1.8
	6 min	4.8	4.3	3.6	2.9	2.3	1.8
B 400	1 min	9.4	8.1	6.6	5.3	4.2	3.4
	1.5 min	8.0	6.8	5.8	4.9	3.9	3.0
	2 min	6.6	5.9	5.1	4.4	3.5	2.7
	2.5 min	5.9	5.1	4.3	3.6	2.9	2.3
	3 min	5.6	5.0	4.2	3.5	2.8	2.1
	3.5 min	5.1	4.6	3.9	3.3	2.6	2.1
	4 min	4.6	4.1	3.6	3.1	2.5	1.9
	5 min	4.5	4.1	3.5	2.9	2.3	1.7
	6 min	4.3	3.8	3.2	2.6	2.1	1.6
B 500	1 min	8.9	7.6	6.2	5.0	4.0	3.2
	1.5 min	7.1	6.2	5.2	4.4	3.6	2.8
	2 min	6.1	5.4	4.7	4.0	3.3	2.5
	2.5 min	5.3	4.7	4.0	3.3	2.7	2.2
	3 min	5.1	4.6	3.9	3.2	2.6	2.1
	3.5 min	4.8	4.3	3.7	3.0	2.5	2.0
	4 min	4.2	3.8	3.4	2.9	2.4	1.8
	5 min	4.2	3.7	3.2	2.7	2.2	1.7
	6 min	3.9	3.5	3.0	2.4	2.0	1.6

Reconstruction Technique	Spheres (mm) / Time	10	13	17	22	28	37
B 600	1 min	8.2	7.1	5.8	4.7	3.8	3.1
	1.5 min	6.6	5.8	4.9	4.1	3.4	2.7
	2 min	5.7	5.1	4.4	3.8	3.1	2.4
	2.5 min	5.0	4.4	3.8	3.1	2.6	2.1
	3 min	4.8	4.3	3.7	3.1	2.5	2.0
	3.5 min	4.4	4.0	3.4	2.9	2.4	1.9
	4 min	3.9	3.6	3.2	2.8	2.3	1.8
	5 min	3.8	3.5	3.0	2.6	2.1	1.7
	6 min	3.6	3.2	2.8	2.3	1.9	1.5
B 1000	1 min	6.6	5.8	4.9	4.0	3.3	2.8
	1.5 min	5.2	4.7	4.1	3.5	2.9	2.4
	2 min	4.7	4.2	3.7	3.2	2.7	2.1
	2.5 min	4.0	3.6	3.2	2.7	2.3	1.9
	3 min	3.9	3.5	3.1	2.6	2.2	1.8
	3.5 min	3.7	3.3	2.9	2.5	2.1	1.8
	4 min	3.3	3.1	2.8	2.4	2.1	1.7
	5 min	3.2	3.0	2.6	2.3	1.9	1.6
	6 min	2.8	2.6	2.3	1.9	1.6	1.4
OSEM	1 min	19.2	14.9	10.9	8.7	7.1	5.9
	1.5 min	17.9	13.6	9.4	7.6	6.1	4.8
	2 min	15.3	12.0	9.2	7.6	5.7	4.6
	2.5 min	13.7	10.4	7.6	6.4	4.9	3.9
	3 min	12.2	9.3	7.0	6.1	4.6	3.3
	3.5 min	11.5	8.6	6.5	5.6	4.3	3.2
	4 min	10.7	8.1	6.3	5.4	4.2	2.9
	5 min	9.5	7.6	6.1	5.1	3.6	2.5
	6 min	8.9	7.5	6.0	4.7	3.4	2.5
C. OSEM	1 min	10.4	8.8	7.1	5.7	4.6	3.7
	1.5 min	8.8	7.5	6.3	5.4	4.5	3.5
	2 min	7.6	6.7	5.8	5.1	4.1	3.0
	2.5 min	6.8	5.9	5.0	4.1	3.2	2.3
	3 min	6.5	5.7	4.8	4.0	3.0	2.2
	3.5 min	5.8	5.1	4.5	3.7	2.9	2.2
	4 min	5.5	4.8	4.1	3.5	2.7	2.0
	5 min	5.3	4.6	3.9	3.2	2.5	1.8
	6 min	5.1	4.4	3.7	3.0	2.3	1.7

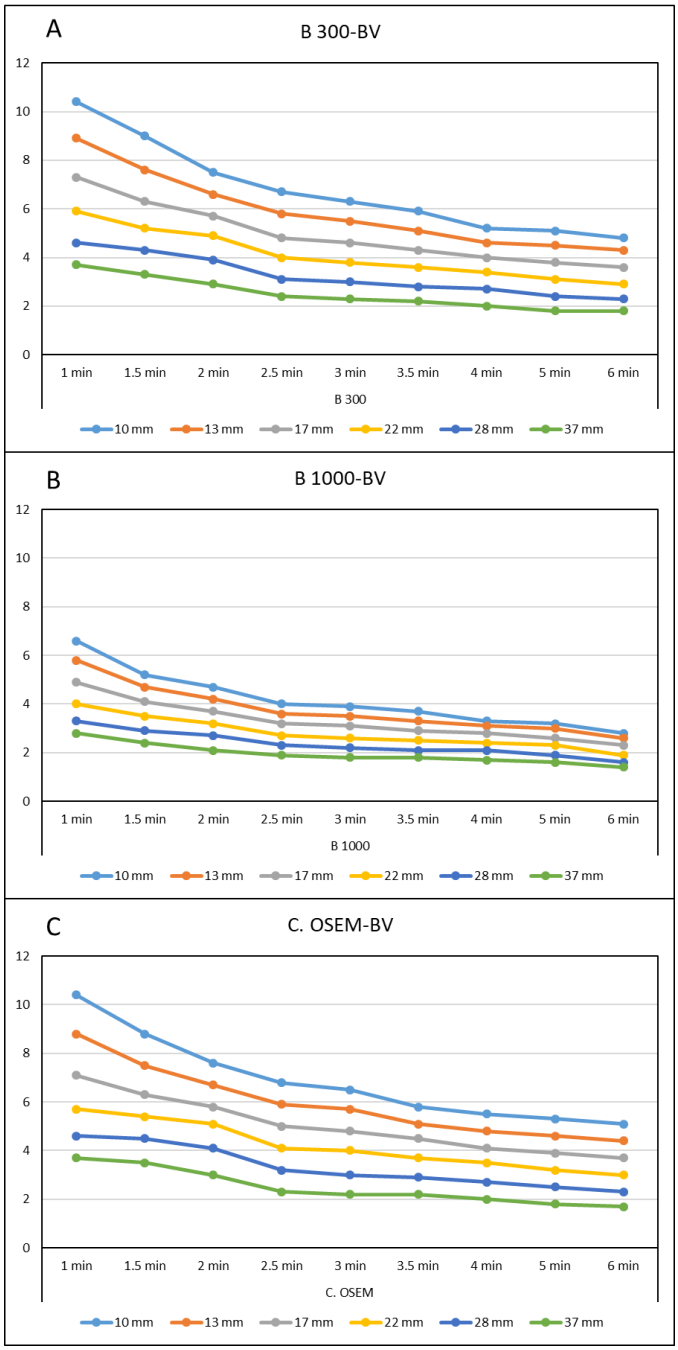

Figure 11. The NEMA IQ phantom BV values for Q. Clear (β = 300 and 1000) and standard reconstruction at various scan times for its different spheres' sizes on the 3-ring PET system. A- PET data reconstructed with Q. Clear with β= 300; B- PET data reconstructed with Q. Clear with β= 1000; C- PET data reconstructed with standard reconstruction technique (OSEM+TOF).

Table 5 encompasses the background variation data of NEMA phantom scanned with the GE Discovery MI PET/CT with a 5-ring detector and reconstructed with various reconstruction techniques and scan times. From Table 4, it is evident that the BV for all spheres decreased while the β-value of the Q. Clear reconstruction techniques increased. Increasing scan time for each reconstruction technique led to decreased BV values for both hot and cold spheres. The 10 mm hot sphere has the highest BV value among all the hot and cold spheres for every reconstruction technique at different scan times. The C. OSEM reconstruction technique has a lower BV compared to the OSEM reconstruction technique for every scan time and all hot and cold spheres. The BV of the C. OSEM reconstruction technique with a scan time of 2.5 minutes was lower than the BV of the Q. Clear reconstruction technique for the β-value of 300, 400, 500, 600, and 1000 at scan times less than 3, 2.5, 2, 2, and 1.5 minutes for all spheres, respectively. Specifically, for the clinical standard reconstruction, the BV value at 2.5 minutes was less than the BV value at 3.5 scan time while it was higher than BV value at 3 minute scan time. Figure 12-A and 12-B represent the background variation data of both hot and cold spheres of the NEMA phantom scanned with the GE PET/CT scanner with a 5-ring detector and reconstructed with Q. Clear reconstruction technique (β = 300 and 1000). Figure 12-C presents the background variation values of each spheres with the clinical standard reconstruction technique and varying scan times.

Table 5. The background variation (BV) present for 5-ring PET/CT scanner of NEMA phantom for hot sphere (10, 13, 17, and 22 mm) and cold sphere (28 and 37 mm) at various scan time (1-6 minutes). The standard reconstruction of the clinic is presented by the bold line around the row. Green shade cells indicate the Lower BV value with the same or lower scan time in compare to the standard reconstruction technique.

Dependency of BV and recon Tech for 5-ring PET scan	Spheres (mm) / Time	10	13	17	22	28	37
B 300	1 min	9.5	7.5	5.9	4.7	3.6	2.6
	1.5 min	8.0	6.4	5.1	4.0	3.1	2.4
	2 min	6.8	5.2	4.0	3.1	2.5	1.9
	2.5 min	5.7	4.5	3.5	2.8	2.3	1.9
	3 min	4.9	4.0	3.2	2.6	2.1	1.7
	3.5 min	4.3	3.4	2.8	2.3	1.9	1.5
	4 min	4.1	3.3	2.8	2.4	2.0	1.5
	5 min	3.5	2.9	2.4	2.2	1.9	1.5
B 400	1 min	7.7	6.3	5.1	4.1	3.2	2.3
	1.5 min	6.5	5.5	4.4	3.5	2.7	2.1
	2 min	5.5	4.5	3.5	2.8	2.2	1.7
	2.5 min	4.6	3.7	3.0	2.5	2.0	1.7
	3 min	3.8	3.2	2.7	2.2	1.8	1.5
	3.5 min	3.3	2.8	2.4	2.0	1.7	1.4
	4 min	2.8	2.5	2.4	2.0	1.7	1.4
	5 min	2.7	2.3	2.1	1.9	1.7	1.4
	6 min	2.8	2.4	2.0	1.9	1.6	1.3
B 500	1 min	6.8	5.7	4.7	3.8	2.9	2.2
	1.5 min	5.8	4.9	4.0	3.2	2.5	2.0
	2 min	4.9	4.0	3.2	2.6	2.1	1.6
	2.5 min	4.0	3.4	2.8	2.3	1.9	1.6
	3 min	3.3	2.9	2.4	2.0	1.7	1.4
	3.5 min	2.8	2.4	2.1	1.8	1.6	1.3
	4 min	2.7	2.4	2.1	1.9	1.6	1.3
	5 min	2.4	2.2	1.9	1.8	1.6	1.3
	6 min	2.6	2.2	1.9	1.7	1.5	1.2
B 600	1 min	6.2	5.2	4.3	3.5	2.7	2.0
	1.5 min	5.2	4.5	3.7	3.0	2.3	1.8
	2 min	4.5	3.7	3.0	2.4	1.9	1.5
	2.5 min	3.8	3.2	2.6	2.2	1.8	1.5
	3 min	3.1	2.7	2.3	1.9	1.6	1.3
	3.5 min	2.7	2.3	2.0	1.8	1.5	1.3
	4 min	2.6	2.4	2.1	1.8	1.5	1.2
	5 min	2.1	1.9	1.8	1.7	1.5	1.2
	6 min	2.4	2.1	1.8	1.7	1.5	1.2

Dependency of BV and recon Tech for 5-ring PET scan	Spheres (mm) / Time	10	13	17	22	28	37
B 1000	1 min	4.7	4.1	3.5	2.9	2.3	1.8
	1.5 min	4.0	3.5	3.0	2.5	2.0	1.6
	2 min	3.5	3.0	2.5	2.1	1.7	1.4
	2.5 min	2.9	2.5	2.2	1.9	1.6	1.3
	3 min	2.5	2.2	1.9	1.6	1.4	1.2
	3.5 min	2.1	1.9	1.7	1.5	1.3	1.1
	4 min	2.0	1.9	1.7	1.5	1.3	1.1
	5 min	1.8	1.7	1.6	1.5	1.3	1.1
	6 min	2.0	1.8	1.6	1.5	1.3	1.1
OSEM	1 min	15.2	10.5	7.9	6.3	5.6	4.2
	1.5 min	14.5	11.0	7.8	5.6	4.6	3.8
	2 min	12.0	8.3	5.7	4.6	3.8	3.0
	2.5 min	10.3	7.3	5.2	4.3	3.5	3.0
	3 min	8.2	6.4	5.3	4.5	3.3	2.8
	3.5 min	7.4	5.9	5.1	4.1	3.2	2.5
	4 min	6.5	5.2	4.6	3.9	3.2	2.4
	5 min	6.4	4.8	4.0	3.6	3.0	2.3
	6 min	5.8	4.2	3.7	3.3	2.6	2.1
C. OSEM	1 min	8.8	7.3	5.8	4.6	3.6	2.8
	1.5 min	7.4	6.2	5.0	4.0	3.1	2.4
	2 min	6.1	5.0	4.0	3.3	2.6	2.0
	2.5 min	5.1	4.2	3.4	2.8	2.3	1.9
	3 min	4.4	3.7	3.0	2.5	2.1	1.8
	3.5 min	5.7	5.0	4.2	3.6	3.0	2.4
	4 min	3.7	3.2	2.7	2.3	1.9	1.5
	5 min	3.1	2.7	2.4	2.1	1.8	1.4
	6 min	5.8	4.2	3.7	3.3	2.6	2.1

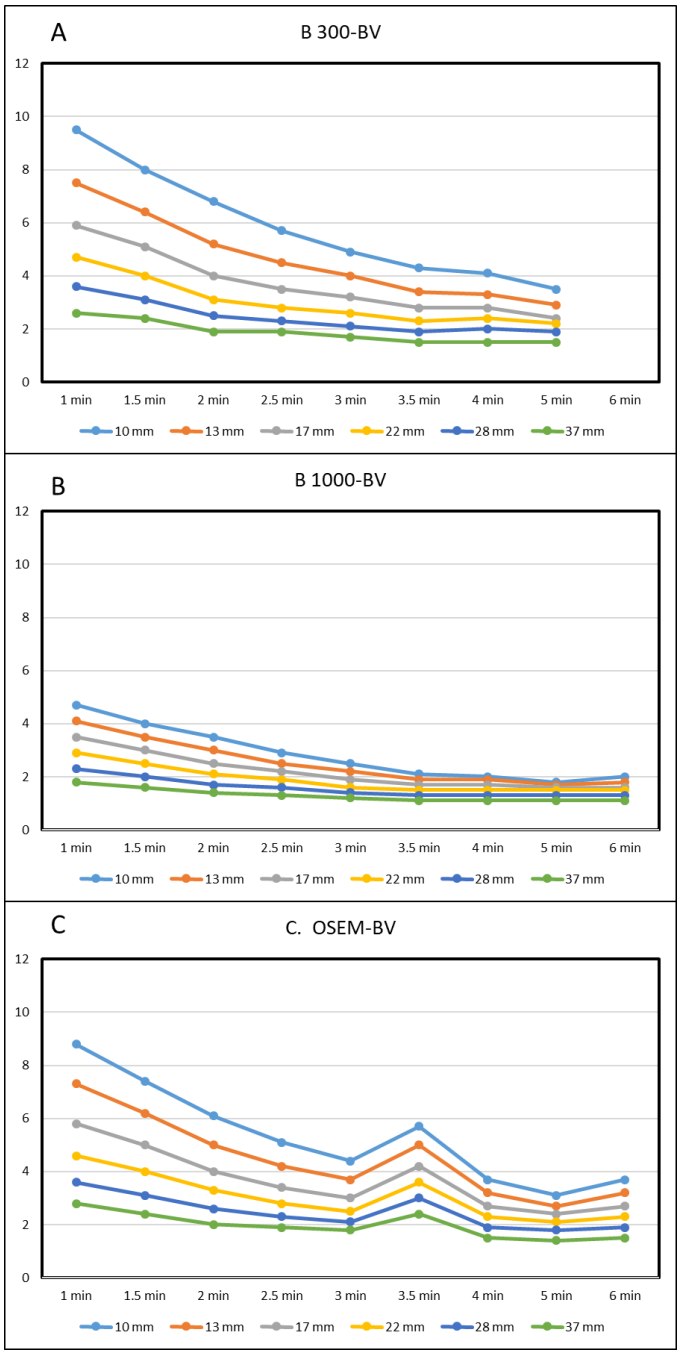

Figure 12. The NEMA IQ phantom BV values for Q. Clear (β = 300 and 1000) and standard reconstruction at various scan times for its different spheres' sizes on the 5-ring PET system. A- PET data reconstructed with Q. Clear with β= 300; B- PET data reconstructed with Q. Clear with β= 1000; C- PET data reconstructed with standard reconstruction technique (OSEM+TOF).

By comparing the BV values of the 3-ring with C. OSEM at 2.5 minutes' scan time vs. 5-ring with the Q. Clear technique for every scan times, the data demonstrates that on average the 5-ring BV values for the Q. Clear reconstruction technique of the 5-ring scanner with β-values of 300, 400, 500, 600, and 1000 is 1.4, 1.8, 1.9, 2.1 and 2.5 lower than the standard reconstruction of 3-ring scanner respectively for the hot spheres. For the cold spheres, the BV values are lower for the Q clear reconstructions with the above-mentioned β-values compared to the C. OSEM reconstruction by 1.3, 1.5, 1.6, 1.7, and 2.0, respectively. The BV values of the 5-ring with OSEM reconstructive technique were similar to the 3-ring with C. OSEM at 2.5 minutes' scan time for both hot and cold spheres at scan time more than 2.5 minute.

5.3 Contrast-to-Noise ratio (CNR)

The CNR for the 3-ring PET/CT system is tabulated in table 6. The CNR as described previously, was calculated by taking the CR to BV ratio for each specific combination of reconstruction technique and scan time. From table 5, the CNR for all spheres decreased with increasing the β-value of the Q. Clear reconstruction technique. Increasing scan time for each reconstruction technique led to an increase in the CNR for both hot and cold spheres. The smallest hot and the largest cold sphere have the lowest and highest CNR value, respectively, among all spheres at any scan time for each reconstruction technique. The C. OSEM reconstruction technique CNR values are higher compared to the OSEM reconstruction for every scan time and all spheres. The CNR of the C. OSEM reconstruction technique at 2.5 minute scan time was similar to the CNR of the Q. Clear reconstructions with all β-values at every scan time at both hot and cold spheres. Figures 13-A and 13-B show the contrast to noise ratio (CNR) data of both hot and cold

spheres of the NEMA phantom scanned with the GE PET/CT scanner with a 3-ring detector and reconstructed with β values of 300 and 100 and the Q. Clear reconstruction technique. Figure 13-C presents the contrast to noise ratio (CNR) value of clinical standard reconstruction technique for each sphere and the varying scan times.

Table 6. The contrast-to-noise ratio (CNR) for the 3-ring PET/CT scanner for hot sphere (10, 13, 17, and 22 mm) and cold sphere (28 and 37 mm) at various scan time (1-6 minutes). The standard reconstruction of the clinic is presented by the bold line around the row. Green shade cells indicate the higher CNR value with the same or lower scan time in compare to the standard reconstruction technique.

CNR =CR/BV 3-ring Reconstruction technique	Spheres (mm) / Time	10	13	17	22	28	37
B 300	1 min	7.0	8.1	8.1	14.2	17.3	23.1
	1.5 min	6.3	9.1	9.7	15.5	19.1	25.8
	2 min	7.3	10.2	10.6	16.1	21.5	29.6
	2.5 min	8.0	11.4	13.5	20.2	26.8	35.5
	3 min	8.0	12.5	13.8	20.9	27.8	36.9
	3.5 min	8.3	13.4	15.1	22.3	29.7	38.6
	4 min	9.2	14.3	16.9	24.0	31.0	42.6
	5 min	9.9	13.8	18.0	26.3	34.4	47.3
	6 min	10.9	14.9	20.0	28.4	36.0	47.4
B 400	1 min	6.9	8.4	9.1	15.5	16.7	24.9
	1.5 min	6.5	9.7	10.6	16.2	20.7	28.1
	2 min	7.5	10.9	11.9	17.8	23.4	31.4
	2.5 min	8.1	12.4	15.0	22.1	28.1	36.6
	3 min	8.0	13.1	15.1	22.5	29.2	40.0
	3.5 min	8.5	14.2	16.5	24.0	31.3	40.0
	4 min	9.3	15.4	18.5	26.1	32.8	44.3
	5 min	10.0	14.6	19.4	27.8	35.3	49.5
	6 min	11.0	16.2	22.3	31.4	38.6	52.7
B 500	1 min	6.5	8.5	9.6	16.3	19.3	26.3
	1.5 min	6.5	10.1	11.8	17.8	22.1	29.8
	2 min	7.3	11.4	12.8	19.4	24.4	33.6
	2.5 min	8.2	12.8	15.9	23.9	29.6	37.8
	3 min	8.0	13.6	16.2	24.3	30.8	39.5
	3.5 min	8.1	14.5	17.2	26.2	32.0	41.5
	4 min	9.1	15.9	19.4	27.6	33.5	46.2
	5 min	9.6	15.6	20.9	29.5	36.1	48.9
	6 min	11.1	17.0	23.5	33.7	39.9	52.0

CNR =CR/BV 3-ring Reconstruction technique	Spheres (mm) / Time	10	13	17	22	28	37
B 600	1 min	6.4	8.6	10.3	17.1	20.0	26.8
	1.5 min	6.4	10.3	12.5	18.9	23.0	30.6
	2 min	7.1	11.5	13.6	20.2	25.5	34.6
	2.5 min	7.9	13.1	16.6	25.2	30.2	39.2
	3 min	7.7	13.9	16.8	24.9	31.5	41.1
	3.5 min	8.2	14.9	18.5	26.9	32.8	43.3
	4 min	8.9	16.1	20.3	28.3	34.3	45.8
	5 min	9.8	15.7	21.9	30.3	37.2	48.5
	6 min	11.1	17.9	24.9	34.7	41.2	54.9
B 1000	1 min	5.8	8.8	11.7	19.2	21.8	28.8
	1.5 min	6.0	10.7	14.2	21.2	25.4	33.2
	2 min	6.3	11.8	15.2	23.1	27.6	38.1
	2.5 min	7.3	13.5	18.5	27.8	32.2	41.8
	3 min	7.1	14.4	18.9	28.5	33.6	44.0
	3.5 min	7.2	15.3	20.4	30.0	35.1	44.0
	4 min	7.8	15.9	21.6	31.8	35.3	46.7
	5 min	8.5	15.7	23.7	33.0	38.7	49.6
	6 min	10.9	19.2	28.6	40.6	46.4	56.7
OSEM	1 min	4.2	4.7	5.0	9.7	11.3	14.4
	1.5 min	3.6	5.0	6.1	11.0	13.9	17.8
	2 min	4.0	5.4	6.1	10.7	15.5	18.9
	2.5 min	4.4	6.2	8.3	13.1	17.9	22.2
	3 min	4.8	7.3	8.7	13.4	19.0	26.1
	3.5 min	4.9	7.9	9.5	14.7	20.3	27.0
	4 min	5.4	7.9	10.4	15.4	20.9	30.0
	5 min	6.2	7.9	11.0	16.2	24.1	35.0
	6 min	6.6	8.1	11.6	17.6	25.4	35.0
C. OSEM	1 min	5.3	7.1	8.1	13.2	15.9	21.9
	1.5 min	5.6	7.8	9.3	14.0	16.9	23.1
	2 min	6.6	8.5	10.3	14.8	18.9	27.1
	2.5 min	7.2	9.7	12.4	18.4	24.2	35.1
	3 min	7.1	10.2	12.8	18.5	25.9	36.7
	3.5 min	7.9	11.5	13.7	20.3	26.8	36.8
	4 min	8.3	11.9	15.4	21.6	28.9	40.5
	5 min	9.2	12.0	16.5	23.7	30.9	45.1
	6 min	9.8	12.7	18.1	25.4	33.8	47.8

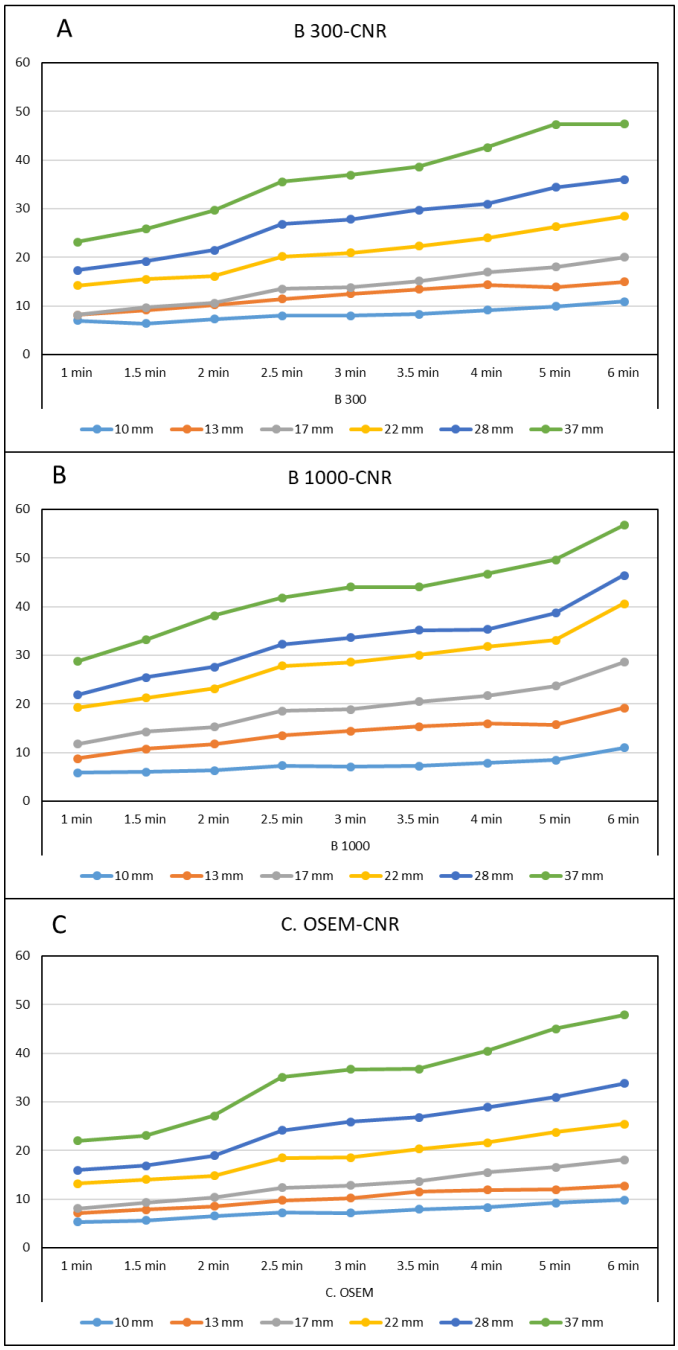

Figure 13. The CNR values for the 3- ring system for every reconstruction technique at various scan times for each sphere size in the NEMA IQ phantom. A- PET data reconstructed with Q. Clear with β= 300; B- PET data reconstructed with Q. Clear with β= 1000; C- PET data reconstructed with standard reconstruction technique (OSEM+TOF).

Table 7 contains the calculated CNR values of the NEMA phantom scanned with the 5-ring scanner. From table 6, the CNR for all spheres increased while the β-value of the Q. Clear reconstruction techniques was increased. Increasing scan time at each reconstruction technique led to an increase in the CNR for both hot and cold spheres. The C. OSEM reconstruction technique has higher CNR than the OSEM reconstruction technique for every scan time and both hot and cold spheres. More specifically, the CNR of the C. OSEM reconstruction technique at 2.5 minutes' scan time was at least 30% higher than the CNR of the OSEM at every scan time and all spheres. The CNR of the C. OSEM reconstruction technique with a 2.5 minute scan time was lower by a factor of 1.2-1.7 times in the hot spheres and 1.1- 1.5 times in the cold spheres than the Q. Clear reconstruction technique with all the β-values and for every scan time. Figures 14-A and 14-B represent the contrast to noise ratio (CNR) data of all spheres of the NEMA phantom scanned with the GE PET/CT scanner with a 5-ring detector and reconstructed with β values of 300 and 100 and the Q. Clear reconstruction technique. Figure 14-C displays the contrast to noise ratio (CNR) values of the clinical standard reconstruction technique for each sphere with varying scan times.

Table 7. The contrast-to-noise ratio (CNR) for the 5-ring PET/CT scanner for hot sphere (10, 13, 17, and 22 mm) and cold sphere (28 and 37 mm) at various scan time (1-6 minutes). The standard reconstruction of the clinic is presented by the bold line around the row. Green shade cells indicate the higher CNR value with the same or lower scan time in compare to the standard reconstruction technique.

CNR =CR/BV 5-ring Reconstruction technique	Spheres (mm) / Time	10	13	17	22	28	37
B 300	1 min	8.7	11.2	15.8	23.0	23.3	34.9
	1.5 min	11.1	13.3	18.1	26.6	27.5	37.8
	2 min	12.7	16.5	23.7	35.4	34.0	47.8
	2.5 min	14.9	19.2	27.2	39.0	37.3	47.7
	3 min	17.8	22.2	29.5	41.8	41.0	53.3
	3.5 min	19.8	26.4	34.4	47.5	45.8	60.2
	4 min	20.5	27.3	34.3	45.0	43.5	60.2
	5 min	24.2	31.9	40.5	49.0	45.8	60.1
B 400	1 min	9.8	12.6	17.6	25.5	25.8	39.0

CNR =CR/BV 5-ring Reconstruction technique	Spheres (mm) / Time	10	13	17	22	28	37
	1.5 min	12.6	14.6	20.3	29.4	31.1	42.7
	2 min	14.4	17.9	26.2	37.8	38.0	53.0
	2.5 min	16.9	21.9	30.6	42.4	42.3	52.8
	3 min	21.0	26.1	33.8	47.8	46.8	59.5
	3.5 min	23.8	30.3	38.6	52.9	50.3	63.6
	4 min	27.5	34.0	39.3	52.3	50.1	63.6
	5 min	28.9	37.9	44.5	55.1	50.1	63.5
	6 min	28.5	38.0	47.6	56.1	53.3	68.5
B 500	1 min	10.5	13.6	18.9	27.3	28.2	40.5
	1.5 min	13.3	16.0	22.2	31.9	33.2	44.5
	2 min	15.3	19.6	28.4	40.3	39.3	55.8
	2.5 min	18.4	23.2	32.5	45.4	43.9	55.6
	3 min	22.9	27.9	37.5	52.1	48.9	63.3
	3.5 min	26.4	34.1	43.5	58.1	52.7	68.0
	4 min	27.0	34.3	43.6	54.5	52.4	68.0
	5 min	30.5	38.3	48.5	57.7	52.5	67.8
	6 min	28.9	40.1	49.4	62.1	56.1	73.6
B 600	1 min	10.9	14.6	20.4	29.4	30.0	44.2
	1.5 min	14.0	16.9	23.7	33.8	35.6	49.1
	2 min	15.8	20.6	30.0	43.3	42.9	59.1
	2.5 min	18.3	23.9	34.5	47.1	45.7	58.9
	3 min	23.0	29.1	38.7	54.3	51.3	67.6
	3.5 min	25.9	34.6	45.2	57.6	55.5	67.5
	4 min	26.6	33.3	43.0	57.0	55.3	73.0
	5 min	32.8	42.9	50.4	61.0	55.4	72.8
	6 min	29.6	40.7	51.4	61.6	55.4	73.0
B 1000	1 min	11.4	16.8	23.9	34.3	33.8	47.6
	1.5 min	14.6	19.6	28.0	39.4	39.2	53.6
	2 min	16.5	22.8	34.4	47.8	45.8	61.4
	2.5 min	19.3	27.4	38.9	52.6	49.1	65.8
	3 min	23.0	31.9	44.5	62.5	56.0	71.1
	3.5 min	26.9	37.2	50.4	66.7	61.0	77.3
	4 min	28.0	37.4	50.4	66.1	60.6	77.2
	5 min	30.4	42.6	53.8	66.2	60.9	77.0
	6 min	29.1	42.5	55.1	67.7	61.2	77.4
OSEM	1 min	4.7	7.2	11.7	16.9	14.8	21.5
	1.5 min	5.7	7.2	11.4	18.5	18.9	24.1
	2 min	6.7	9.5	16.0	23.2	22.9	30.7
	2.5 min	7.6	10.9	17.7	25.1	25.3	30.7

CNR =CR/BV 5-ring Reconstruction technique	Spheres (mm) / Time	10	13	17	22	28	37
	3 min	9.8	12.8	17.2	23.6	26.9	32.7
	3.5 min	10.6	14.3	18.3	26.2	28.3	36.6
	4 min	11.9	16.4	20.3	27.1	28.2	38.2
	5 min	12.5	18.5	23.8	29.5	30.0	39.9
	6 min	13.9	21.3	25.3	32.1	34.5	43.6
C. OSEM	1 min	7.0	9.5	13.7	21.5	21.4	30.1
	1.5 min	9.3	11.5	15.5	24.5	25.3	35.3
	2 min	11.0	14.0	19.9	30.7	29.9	42.6
	2.5 min	13.1	16.9	23.6	35.6	34.1	44.5
	3 min	15.7	19.6	26.7	39.7	37.3	46.8
	3.5 min	13.6	16.1	19.7	28.3	26.6	35.0
	4 min	18.0	23.3	30.0	42.7	41.6	56.0
	5 min	21.8	28.4	34.2	47.0	43.9	59.8
	6 min	21.8	28.0	34.6	46.0	47.3	61.0

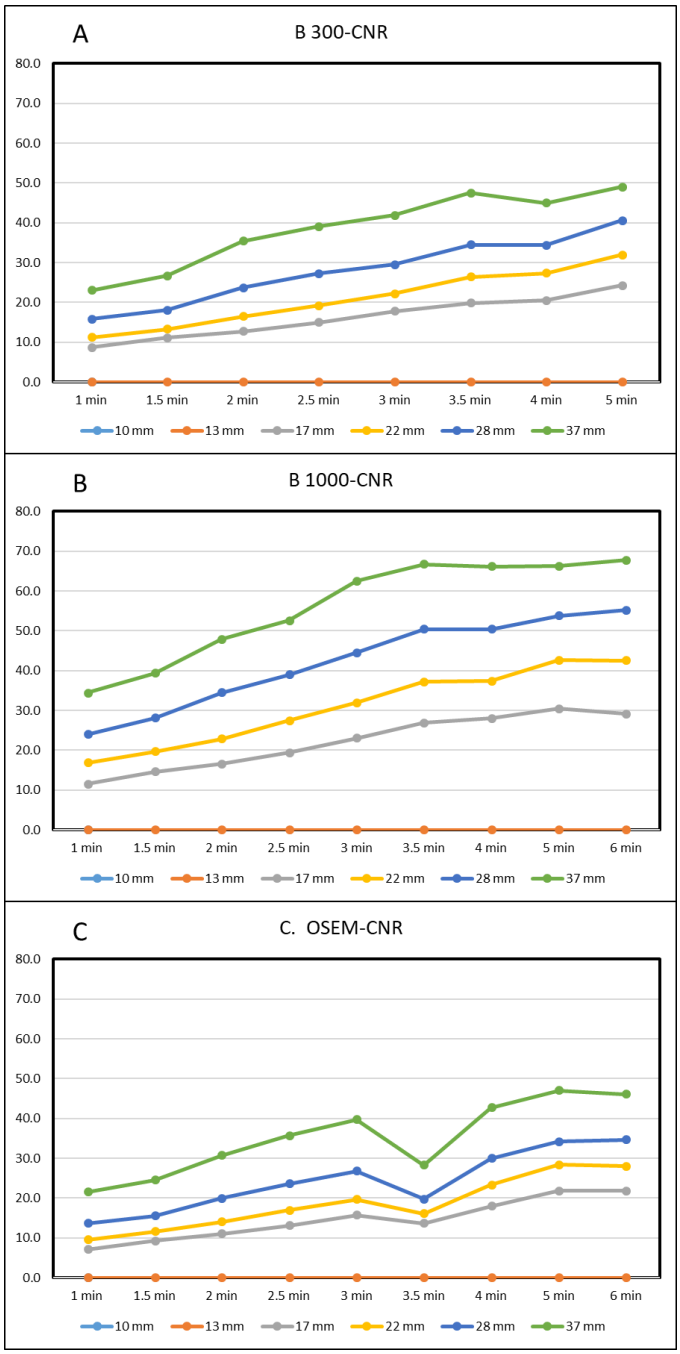

Figure 14. The CNR values for the 5- ring system for every reconstruction technique at various scan times for each sphere size in the NEMA IQ phantom. A- PET data reconstructed with Q. Clear with β= 300; B- PET data reconstructed with Q. Clear with β= 1000; C- PET data reconstructed with standard reconstruction technique (OSEM+TOF).

On average, the CNRs of the Q. Clear reconstruction for every β values at various scan times on the 5-ring system was 2.2-3.2 times higher than the 2.5 minute C. OSEM reconstruction on the

3-ring system for all the hot spheres. This same comparison applied for cold spheres, illustrates that on overage the CNRs of the Q. Clear for every β value at various scan times of the 5-ring system was 1.5-2 times higher than the 3-ring system with C. OSEM and a scan time of 2.5 minutes. The CNR of the 5-ring with OSEM reconstructive technique was approximately 1.4 and 1.1 higher than the 2.5 minute C. OSEM reconstruction on the 3 ring system for both hot and cold spheres respectively at every scan time.

Figure 15-A, 15-B, 15-C represent the CR, BV, and CNR variation of NEMA phantom scanned with the GE PET/CT scanner with a 5-ring detector reconstructed with C. OSEM at various scan time and with the GE PET/CT scanner with a 3-ring detector reconstructed with C. OSEM at 2.5 min/bp. In 5-ring, CR and CNR values were higher than the 3-ring with 1.5, 2, and 2.5 min/bp for all spheres, but the BV values were less than the 3-ring with 2 and 2.5 min/bp for all spheres. By this comparison, it seems that the C. OSEM with 2 min/bp on the 5-ring detector, image quality parameters including CR, BV, and CNR were higher than the C. OSEM with 2.5 min/bp on 3-ring detector.

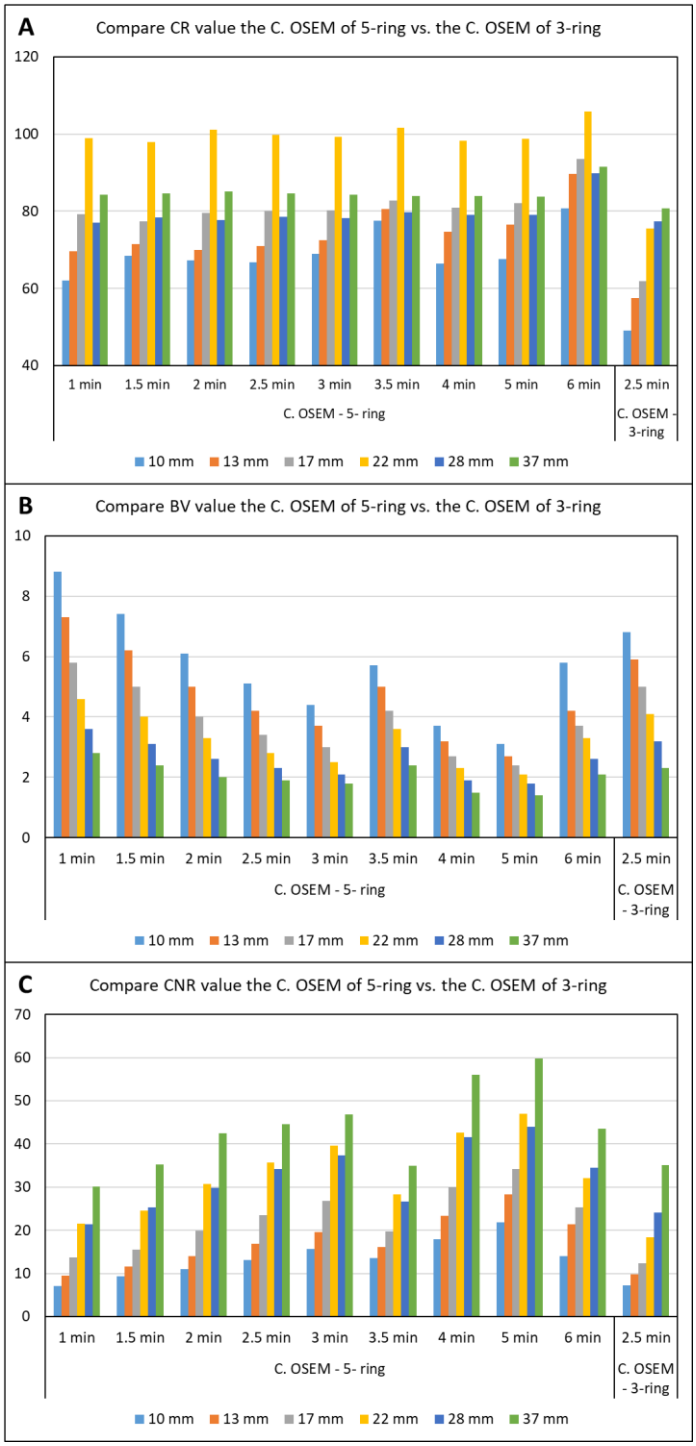

Figure 15. This illustrates the image quality parameters including CR, BV, and CNR for scanner with 5-ring detector by C. OSEM reconstruction technique at various scan time in compare to the 3-ring scanner with C. OSEM at 2.5 min/bp for all spheres of NEMA phantom.

6. Discussion

The purpose of this study was to investigate the impact of the Q-Clear reconstruction technique on the image quality of PET data of both GE Discovery MI PET/CT units installed at Oregon Health and Science University (OHSU) and to evaluate the possibility of decreasing scan time (or injected activity) at both systems. The NEMA phantom was scanned on both scanners with the specific activity at a scan time and reconstruction technique (OSEM: iteration 4, subset 34, and post-processing filter of 2 mm) based on the provided NEMA Testing document from the vendor. The data was reconstructed with our clinical reconstruction technique (OSEM: iteration 4, subset 16, and post-processing filter of 5 mm + TOF) at 2.5 min/bp as our standard reconstruction technique in order to establish a baseline for image quality parameters, including contrast recovery (CR), background variation (BV), and contrast-to-noise ratio (CNR). Based on the literature review, the range of penalty factor (β) for the Q-Clear technique chosen for this study was 300, 400, 500, 600, and 1000. The initial scan protocol on the NEMA phantom used the scan time of 6 min/bp as simulated reconstructions could not be completed with longer scan times than the initial actual phantom scan. As we also aimed to evaluate the possibility of decreasing the scan time, the data were reconstructed at various scan times 1-6 min for every reconstruction technique.

These two scanners have a different axial field-of-view (AFOV) of 15 and 25 cm as one of them has a 3-ring detector and the other has a 5-ring detector. The advantage of larger AFOV includes better image quality, higher sensitivity, and lower scan time or administered activity to the patient (6). Our results were alongside the previous study, and the image quality parameters were higher on the PET/CT scanner with the 5-ring detector. The CR and CNR of the 5-ring scanner were higher than the 3-ring for every reconstruction technique at various scan times. Also,

the BV of the 5-ring was lower than the 3-ring for every reconstruction technique at different scan times. Our result showed that the overall performance of a PET/CT scanner with a 5-ring is higher than the scanner with a 3-ring, agreeing with previous studies (39).

Our results on the 3-ring scanner showed that increasing the β value from 300 to 1000 with Q. Clear, led to a decrease in the CR of the smallest hot lesion (13 mm) by 57% on average over various scan times due to the higher smoothing with higher β value. On the 5-ring scanner, increasing the β value from 300 to 1000 led to the CR of the smallest hot lesion (13 mm) decreasing by approximately 34% on average over various scan times due to the higher smoothing with the higher β value. This comparison between these two scanners illustrates that the higher sensitivity of a 5-ring detector can decrease the effect of smoothing with high β values. The data presented on the 3-ring showed that the BV decreased 30% on average over various scan times for both hot and cold lesions when the β value increased from 300 to 1000 due to controlling noise with higher β values. On the 5-ring scanner, the BV decreased by 50% on average over the same scan times and β value range as for the 3-ring scanner. The comparison between these two scanners based on the CR and BV values shows evidence that the scanner with higher sensitivity (larger AFOV) helps decrease the noise in the image and provides better CR for PET image data.

The comparison of CNR on both 3- and 5-ring scanners represented the different trends. On a 3-ring, although increasing β value from 300 to 1000 led to a decrease in the CR and BV, but the CNR increased by increasing the scan time on the hot and cold lesions. On a 5-ring detector, the same trends of CNR on a 3-ring, and with scan time more than 3.5 min/bp, the slope of increasing CNR decreased. This might be due to the noise suppression because of longer scan time and higher smoothing data.

The other purpose of this study was to evaluate the possibility of decreasing scan time (or injected activity) for both systems. From a previous study (42), the custom-designed phantom was scanned on a GE PET/CT scanner with AFOV of 20 cm with ^{18}F-NaF and β range of 200-700 with scan times of 30-120 second and the SNR and CV was evaluated. This previous study used Q-Clear with a β value of 400 and 1.5 min/bp (25% less than their routine scan time, 2 min), and they achieved 24% and 18% higher SNR and contrast in compared to the OSEM reconstruction technique. Our results indicate that lowering scan time (or injected activity) might not be appropriate on the 3-ring scanner since the CR and CNR were not improved with Q-Clear technique at scan time less than 2.5 min/bp compared to our current clinical OSEM reconstruction technique. However, on the 5-ring scanner, there is an opportunity to lower scan time by 20% (from 2.5 to 2 min/bp) when the Q-Clear with β value of 500 and 600 was used with scan time of 2 and 2.5 min/bp in compared to the standard OSEM on this scanner. The comparison of the standard reconstruction technique on the 3-ring detector scanner with the 5-ring detector scanner using Q-Clear reconstruction technique illustrates that the Q-Clear with β value of 300, 400, 500, 600, and 1000 and scan times of 2 and 2.5 minutes provided higher CR and CNR and lower BV.

7. Conclusion

Although it seems the standard image reconstruction technique on a 3-ring detector scanner is optimized, we can suggest that on a PET/CT with a 5-ring detector, the Q-Clear with β value of 500 with a scan time of 2 min/bp can provide higher CR, BV, and CNR than the CR, BV, and CNR that reconstructed by C. OSEM on both scanners. However, different clinical image representation is possible using Q. Clear on one scanner and not the other, which would be unacceptable to the interpreting physicians. For this reason, maintaining the C. OSEM technique on the 5-ring scanner would be preferable and as shown with the phantom data, it would allow for a decrease in scan time while maintaining the CNR levels of the 3-ring scanner.

8. Limitation and Future Work

A limitation of this study was the limited time frame and high workload of the PET/CT in the clinic, making it difficult to obtain more data on the two PET/CT scanners. Another limitation was the time-consuming aspect of simulating every image reconstruction technique in addition to running the NEMA IQ evaluation software on the reconstructed data on the GE system.

To expand on this current research, future work of this study could include the evaluation of other β values in phantom image data, and the evaluation of the effect of Q-Clear on the patient images with ^{18}F-FDG along with different radionuclides with radiologist experts scoring the image quality. Furthermore inventigation would be pair this quantitive analysis of CNR, CR, and BV with the NEMA phantom with an observer study that the clinical image assessment based on scoring images to determine the acceptable image quality with Q. Clear reconstruction technique in the clinic. Addition to that, the observer study is suggested to investigate the visual assessment of images that reconstrusted with Q. Clear and C. OSEM to evaluate the difference these two for the observer. Lastly, the number of counts for the acceptable image quality could be determined for both scanners (GE PET/CT with 3- and 5-ring) then based on that the amount of administerted activity or scan time would be defined.

9. References

1. Gray JE, Barnes GT, Bronskill MJ. The role of the clinical medical physicist in diagnostic radiology. AAPM Task Group. 1994;42.
2. Mawlawi O, Townsend DW. Multimodality imaging: an update on PET/CT technology. European journal of nuclear medicine and molecular imaging. 2009;36(1):15-29.
3. Czernin J, Phelps ME. Positron emission tomography scanning: current and future applications. Annual review of medicine. 2002;53(1):89-112.
4. Teoh EJ, McGowan DR, Bradley KM, Belcher E, Black E, Gleeson FV. Novel penalised likelihood reconstruction of PET in the assessment of histologically verified small pulmonary nodules. European radiology. 2016;26(2):576-84.
5. Teoh EJ, McGowan DR, Bradley KM, Belcher E, Black E, Moore A, et al. 18F-FDG PET/CT assessment of histopathologically confirmed mediastinal lymph nodes in non-small cell lung cancer using a penalised likelihood reconstruction. European radiology. 2016;26(11):4098-106.
6. Pan T, Einstein SA, Kappadath SC, Grogg KS, Lois Gomez C, Alessio AM, et al. Performance evaluation of the 5-Ring GE Discovery MI PET/CT system using the national electrical manufacturers association NU 2-2012 Standard. Medical physics. 2019;46(7):3025-33.
7. Surti S, Viswanath V, Daube-Witherspoon ME, Conti M, Casey ME, Karp JS. Benefit of improved performance with state-of-the art digital PET/CT for lesion detection in oncology. Journal of Nuclear Medicine. 2020;61(11):1684-90.
8. Budinger TF, Derenzo SE, Gullberg GT, Greenberg WL, Huesman RH. Emission computer assisted tomography with single-photon and positron annihilation photon emitters. Journal of computer assisted tomography. 1977;1(1):131-45.
9. Zhang J, Maniawski P, Knopp MV. Performance evaluation of the next generation solid-state digital photon counting PET/CT system. EJNMMI research. 2018;8(1):1-16.
10. Van Sluis J, De Jong J, Schaar J, Noordzij W, Van Snick P, Dierckx R, et al. Performance characteristics of the digital biograph vision PET/CT system. Journal of Nuclear Medicine. 2019;60(7):1031-6.
11. Conti M. Focus on time-of-flight PET: the benefits of improved time resolution. European journal of nuclear medicine and molecular imaging. 2011;38(6):1147-57.
12. Akamatsu G, Mitsumoto K, Taniguchi T, Tsutsui Y, Baba S, Sasaki M. Influences of point-spread function and time-of-flight reconstructions on standardized uptake value of lymph node metastases in FDG-PET. European journal of radiology. 2014;83(1):226-30.
13. Rapisarda E, Bettinardi V, Thielemans K, Gilardi M. Image-based point spread function implementation in a fully 3D OSEM reconstruction algorithm for PET. Physics in medicine & biology. 2010;55(14):4131.
14. Armstrong IS, Kelly MD, Williams HA, Matthews JC. Impact of point spread function modelling and time of flight on FDG uptake measurements in lung lesions using alternative filtering strategies. EJNMMI physics. 2014;1(1):1-18.
15. Rogasch JM, Suleiman S, Hofheinz F, Bluemel S, Lukas M, Amthauer H, et al. Reconstructed spatial resolution and contrast recovery with Bayesian penalized likelihood reconstruction (Q. Clear) for FDG-PET compared to time-of-flight (TOF) with point spread function (PSF). EJNMMI physics. 2020;7(1):1-14.

16. Nuyts J, Beque D, Dupont P, Mortelmans L. A concave prior penalizing relative differences for maximum-a-posteriori reconstruction in emission tomography. IEEE Transactions on nuclear science. 2002;49(1):56-60.
17. Asma E, Ahn S, Ross SG, Chen A, Manjeshwar RM, editors. Accurate and consistent lesion quantitation with clinically acceptable penalized likelihood images. 2012 IEEE Nuclear science symposium and medical imaging conference record (NSS/MIC); 2012: IEEE.
18. Ahn S, Fessler JA. Globally convergent image reconstruction for emission tomography using relaxed ordered subsets algorithms. IEEE transactions on medical imaging. 2003;22(5):613-26.
19. Ross S. Q.Clear. GE Healthcare White paper. 2013.
20. Jaskowiak CJ, Bianco JA, Perlman SB, Fine JP. Influence of reconstruction iterations on 18F-FDG PET/CT standardized uptake values. Journal of Nuclear Medicine. 2005;46(3):424-8.
21. Surti S, Pantel AR, Karp JS. Total body PET: why, how, what for? IEEE Transactions on Radiation and Plasma Medical Sciences. 2020;4(3):283-92.
22. Jones T, Townsend DW. History and future technical innovation in positron emission tomography. Journal of Medical Imaging. 2017;4(1):011013.
23. Jones T. The role of positron emission tomography within the spectrum of medical imaging. European journal of nuclear medicine. 1996;23(2):207-11.
24. Bushberg JT, Boone JM. The essential physics of medical imaging: Lippincott Williams & Wilkins; 2011.
25. Association NEM, NEMA N. NU 2-2018: performance measurements of positron emission tomographs (PET). Rosslyn: National Electrical Manufacturers Association. 2018.
26. Christian PE, Waterstram-Rich KM. Nuclear medicine and PET/CT: technology and techniques: Mosby/Elsevier; 2007.
27. Teoh EJ, McGowan DR, Schuster DM, Tsakok MT, Gleeson FV, Bradley KM. Bayesian penalised likelihood reconstruction (Q. Clear) of 18F-fluciclovine PET for imaging of recurrent prostate cancer: semi-quantitative and clinical evaluation. The British journal of radiology. 2018;91(1085):20170727.
28. Texte E, Gouel P, Thureau S, Lequesne J, Barres B, Edet-Sanson A, et al. Impact of the Bayesian penalized likelihood algorithm (Q. Clear®) in comparison with the OSEM reconstruction on low contrast PET hypoxic images. EJNMMI physics. 2020;7:1-15.
29. Shepp LA, Vardi Y. Maximum likelihood reconstruction for emission tomography. IEEE transactions on medical imaging. 1982;1(2):113-22.
30. Hudson HM, Larkin RS. Accelerated image reconstruction using ordered subsets of projection data. IEEE transactions on medical imaging. 1994;13(4):601-9.
31. Veklerov E, Llacer J. Stopping rule for the MLE algorithm based on statistical hypothesis testing. IEEE Transactions on Medical Imaging. 1987;6(4):313-9.
32. Mumcuoglu EÜ, Leahy RM, Cherry SR. Bayesian reconstruction of PET images: methodology and performance analysis. Physics in Medicine & Biology. 1996;41(9):1777.
33. Chen L, Chen D, Huang T, Lou C. The Impact of Bayesian Penalized Likelihood Reconstruction Algorithm on Quantitative Accuracy of Positron Emission Tomography Volumetric Measurements. 2020.
34. De Pierro AR, Yamagishi MB. Fast EM-like methods for maximum" a posteriori" estimates in emission tomography. IEEE transactions on medical imaging. 2001;20(4):280-8.

35. Chicheportiche A, Goshen E, Godefroy J, Grozinsky-Glasberg S, Oleinikov K, Meirovitz A, et al. Can a penalized-likelihood estimation algorithm be used to reduce the injected dose or the acquisition time in 68 Ga-DOTATATE PET/CT studies? EJNMMI physics. 2021;8(1):1-17.
36. Bettinardi V, Presotto L, Rapisarda E, Picchio M, Gianolli L, Gilardi M. Physical Performance of the new hybrid PET/CT Discovery-690. Medical physics. 2011;38(10):5394-411.
37. Association NEM. Performance measurements of positron emission tomographs. NEMA standards publication NU 2-2001. 2001.
38. Teoh EJ, McGowan DR, Macpherson RE, Bradley KM, Gleeson FV. Phantom and clinical evaluation of the Bayesian penalized likelihood reconstruction algorithm Q. Clear on an LYSO PET/CT system. Journal of Nuclear Medicine. 2015;56(9):1447-52.
39. Reynés-Llompart G, Gámez-Cenzano C, Romero-Zayas I, Rodríguez-Bel L, Vercher-Conejero JL, Martí-Climent JM. Performance characteristics of the whole-body discovery IQ PET/CT system. Journal of Nuclear Medicine. 2017;58(7):1155-61.
40. Wyrzykowski M, Siminiak N, Kaźmierczak M, Ruchała M, Czepczyński R. Impact of the Q. Clear reconstruction algorithm on the interpretation of PET/CT images in patients with lymphoma. EJNMMI research. 2020;10(1):1-8.
41. Morzenti S, De Ponti E, Guerra L, Zorz A, Landoni C, Crivellaro C, et al. Performance evaluation of the Discovery IQ-GE PET/CT scanner according to NEMA NU2-2012 standard. Journal of Nuclear Medicine. 2015;56(supplement 3):1846-.
42. Yoshii T, Miwa K, Yamaguchi M, Shimada K, Wagatsuma K, Yamao T, et al. Optimization of a Bayesian penalized likelihood algorithm (Q. Clear) for 18 F-NaF bone PET/CT images acquired over shorter durations using a custom-designed phantom. EJNMMI physics. 2020;7(1):1-14.